MR. COOPER D. STACEY (Orcid ID : 0000-0003-0294-5609)

Article type : Original Manuscript

How turbidity current frequency and character varies down a fjord-delta system: Combining direct monitoring, deposits and seismic data

COOPER D. STACEY*, PHILIP R. HILL*, PETER J. TALLING†, RANDOLPH J. ENKIN* and JOHN HUGHES CLARKE‡, D. GWYN LINTERN*

*Natural Resources Canada, Geological Survey of Canada, P.O. Box 6000, Sidney, B.C., V8L 4B2, Canada (E-mail: cooper.stacey@canada.ca)

†Departments of Earth Sciences and Geography, University of Durham, Durham, DH1 3LY, U.K.

‡Centre for Coastal & Ocean Mapping, University of New Hampshire, 24 Colovos rd., Durham, New Hampshire, USA 03824.

Associate Editor – Jaco Baas

Short Title – Turbidity currents: linking monitoring to deposits

This is an Accepted Article that has been peer-reviewed and approved for publication in the *Sedimentology*, but has yet to undergo copy-editing and proof correction. Please cite this article as an "Accepted Article"; doi: 10.1111/sed.12488

ABSTRACT

Submarine turbidity currents are one of the most important processes for moving sediment across our planet; they are hazardous to offshore infrastructure, deposit petroleum reservoirs worldwide, and may record tsunamigenic landslides. However, there are few studies that have monitored these submarine flows in action, and even fewer studies that have combined direct monitoring with longer-term records from core and seismic data of deposits. This study provides one of the most complete studies yet of a turbidity current system. The aim here is to understand what controls changes in flow frequency and character along the turbidite system. The study area is a 12 km long delta-fed fjord (Howe Sound) in British Columbia, Canada. Over 100 often powerful (up to 2 to 3 m/s) events occur each year in the highly-active proximal channels, which extend for 1 to 2 km from the delta lip. About half of these events reach the lobes at the channel mouths. However, flow frequency decreases rapidly once these initially sand-rich flows become unconfined, and only one to five flows run out across the mid-slope each year. Many of these sand-rich, channelized, delta-sourced flows therefore dissipated over a few hundred metres, once unconfined, rather than eroding and igniting. Upflow migrating bedforms indicate that supercritical flow dominated in the proximal channels and lobes, and also across the unconfined mid-slope. These supercritical flows deposited thick sand beds in proximal channels and lobes, but thinner and finer beds on the unconfined mid-slope. The distal flat basin records far larger volume and more hazardous events that have a recurrence interval of *ca* 100 years. This study shows how sand-rich delta-fed flows dissipate rapidly once they become unconfined, that supercritical flows dominate in both confined and unconfined settings, and how a second type of more hazardous, and much less frequent events are linked to a different scale of margin failure.

INTRODUCTION

Turbidity currents dominate sediment transport into many parts of the ocean. These often powerful flows can badly damage offshore infrastructure, such as pipelines, or break networks of submarine telecommunication cables that now carry >95% of global data traffic (Heezen & Ewing, 1952; Carter et al., 2014; Cooper et al., 2013). Their deposits (turbidites) host important petroleum reserves in many locations worldwide (Nielsen et al., 2008), and could potentially provide a valuable long-term record of tsunamigenic landslides or major earthquakes that threaten coastal areas (Goldfinger et al., 2010; Atwater et al., 2014; Mountjoy et al., 2018). Only terrestrial river systems disperse such large volumes sediment over such large areas of the planet (Talling et al., 2014).

However, in contrast to the many thousands of direct observations from rivers, there are very few direct observations from active turbidity currents (Inman et al., 1978; Prior et al., 1987; Xu et al., 2013; Talling et al., 2014; Lintern et al., 2016; Hughes Clarke, 2016; Azpiroz-Zabala et al., 2017). This study uses flow monitoring data from previous work at Howe Sound in British Columbia, Canada, which includes some of the most detailed measurements yet made from within turbidity currents (Hughes Clarke et al., 2012, 2013; Hughes Clarke, 2016). However, in most locations worldwide, the only record of turbidity currents are the deposits they leave behind. Indeed, it may be impossible to measure the more infrequent types of turbidity current over the timescales of most research projects (<1 to 10 years). It is therefore important to link direct monitoring observations and flow deposits (Talling et al., 2015; Fildani et al., 2017; Hage et al., 2018). Even fewer monitoring studies have gone on to combine such direct flow observations with information from deposits (e.g. Prior et al., 1987; Zeng et al., 1991; Paull et al., 2005, 2010a; Crookshanks &

Gilbert, 2008; Symons et al., 2016; Hizzett et al., 2017; Hage et al., in press), or sediment trap samples from within the flow (e.g. Liu et al., 2008; Xu et al., 2010). These studies have tended to study a small number of locations along a small part of the full flow pathway. This contribution presents probably the most complete study yet that combines monitoring, cores and seismic data of deposits from delta shoreline to sink. This study provides a valuable new view into turbidity current systems, and allows for new insights into offshore and coastal geohazards.

The main focus of this study is on how the frequency and character of turbidity currents varies with distance down system, and what factors control those variations. In particular, how seabed geomorphology affects flow behaviour is discussed. This work seeks to understand where and why flows dissipate (and the length scales over which this occurs), where and why flows are subcritical or supercritical, and whether flow frequency and runout is a continuum or bimodal. Understanding turbidity current frequency, and how it changes with distance, is particularly important for assessing hazards to seabed infrastructure (Cooper et al., 2012). Changes in flow frequency are also key for understanding fundamental flow behaviour; such as how often flows erode and accelerate (ignite; Parker et al., 1982), or deposit sediment and dissipate, and the length scales over which such changes occur. It has also been proposed that turbidity currents in larger submarine canyon fed systems are strongly bimodal, such that most events are canyon filling, whilst only a few much larger flows flush sediment out of canyons (Arzola et al., 2008; Allin et al., 2016). More generally, flow frequency has important implications for the tempo of organic carbon and nutrient transport into deeper water (Galy et al., 2007) and the physical disturbance of benthic ecosystems (Paull et al., 2010b). The frequency and

magnitude of sediment and water discharge has long been a key subject for terrestrial river systems (Wolman & Miller, 1960), and this study is one of the initial steps towards measuring magnitude-frequency relations of submarine turbidity currents.

Ancient turbidity current deposits have been used to understand the character and frequency of potentially hazardous triggering mechanisms, such as earthquakes, submarine slope failures and associated tsunamis (Adams, 1990; Goldfinger, 2011; Hunt et al., 2011; Atwater et al., 2014; Arai et al., 2013; Clare et al., 2014; Mountjoy et al., 2018). Such marine turbidite records are potentially valuable because they extend farther back in time than most terrestrial information, for instance historical records of major earthquakes. However, there is often uncertainty as to whether turbidites faithfully record such hazardous events or if they show an incomplete history (Goldfinger et al., 2011; Sumner et al., 2012; Atwater & Griggs, 2014). A motivation for this study is therefore to understand records of tsunamigenic slope failure, or major river-floods (Table 1).

STUDY AREA: SQUAMISH DELTA AND HOWE SOUND

Howe Sound is a marine fjord located *ca* 50 km north of Vancouver in British Columbia, Canada. The Squamish River enters the head of the fjord to produce a delta system, whose proximal part comprises a series of channels that extend for *ca* 1.5 km to water depths of *ca* 150 m (Fig. 1A and B; Hughes Clarke et al., 2014). The channel floors are characterized by upslope-migrating bedforms (Hughes Clarke, 2016; Hizzett et al., 2017; Hage et al., 2018). Flows that expand at the channel mouths have created a series of lobes characterized by active bedforms (Fig. 1B). The basin extends for *ca* 15 km south to a large glacial moraine

called the Porteau Cove Sill that was emplaced at 12.9 ka (Armstrong, 1981). The sill rises steeply from a depth of 280 to 35 m below sea level (mbsl) (Fig. 1A). Several smaller rivers enter Howe Sound and create smaller-scale fans, the most notable being Britannia Creek (Fig. 1C).

Water discharge from the Squamish River increases from *ca* 100 m^3/s during the winter, to *ca* 500 m^3/s during a four-month summer freshet period, primarily due to snow melt. Turbidity current activity tends to initiate with discharges in excess of 300 to 350 m^3 (Hughes Clarke, 2013; Clare et al., 2016). Occasional sharp peaks in river discharge reach *ca* 1000 m^3/s during the freshet (Hughes Clarke et al., 2012). The suspended sediment concentration in the river water is low (with <0.2% volume or 5 g/litre; Hickin, 1989). Around 10^6 m^3 of sediment are delivered annually to the delta by the river, primarily through suspension settling (Hickin, 1989). This compares to sediment volumes of 2×10^4 m^3 to 15×10^4 m^3 for the five largest delta-lip failures observed in 2011 (Hughes Clarke et al., 2012, 2013). The river generates a sediment-laden surface plume with grain sizes ranging from sand to clay with generally only silt and clay extending beyond the Porteau Cove Sill (Syvitski & Murray, 1981). The surface plume is relatively dilute with measured sediment concentrations of <0.03% by volume (Hughes Clarke et al., 2012). The river discharge does not plunge directly to form hyperpycnal flows (Hughes Clarke, 2016). The sea floor sediment for the first few hundred metres seaward of the delta lip is characterized by fine to medium sands and silt (Hage et al., 2018), while the mid-slope and basin are characterized by silt and clay, respectively (Syvitski & MacDonald, 1982).

The Squamish Delta has been affected by human activity, in particular by diversion of the main river in 1971 by a training dyke (Hickin, 1989). Previously, the Squamish River was located further to the south-east, at the abandoned position of the Mamquan River (see Fig. 1B). As subsequently discussed, the delta-system may therefore still be evolving after that forced avulsion 47 years ago (Hughes Clarke et al., 2014). A relict submarine channel extends for *ca* 2.5 km from the Mamquam River. This relict channel may have once connected to elongate depressions that occur 5 km from the delta (Fig. 1A). The position of the main active channel in the current (post 1921 flood and channel avulsion – see Table 1) Squamish River also migrates. This can also lead to marked changes in activity within three offshore channels that are cut into the delta front (Hughes Clarke, 2012, 2013, 2016).

Britannia Creek mining influence

Britannia Creek enters the eastern side of the fjord, around 8 km from the Squamish Delta, and was the site of a copper and zinc mine that operated from 1898 to 1974 (Fig. 1C). During that time approximately 40 million tonnes of tailings enriched in gold, and sulphides of iron, copper, zinc, lead and silver were disposed of into the marine environment at the Britannia Mine (Ellis & Popham, 1983). Most of the sulphides are believed to have been transported by mass transport of contaminated materials from Britannia Fan directly to the adjacent sea floor or by adhesion to fine sediments and dispersal throughout the upper Howe Sound Basin (Drysdale, 1990). Once in the marine environment, tailings rich in sulphides were transported north as far as Watts Point, and as far as the Porteau Cove Sill to the south (Fig. 1) (Thompson & McComas, 1974; Syvitski & MacDonald, 1982; Drysdale, 1990). Acid mine drainage also resulted in high concentrations of dissolved copper in the Britannia Creek area through molecular diffusion (Thompson & Terrence, 1977; Drysdale,

1991; Steffen Robertson & Kristen, 1991; EVS Environmental Consultants, 1997). It is subsequently demonstrated that this input produced a discernible geochemical signature in the fjord sediments that is used for dating.

SUMMARY OF PREVIOUS DIRECT MONITORING OF FLOW PROCESSES

Previous direct monitoring of Howe Sound included a series of 93 time-lapse multibeam bathymetric surveys collected from the proximal part of the Squamish Delta every weekday from May to September in 2011 (Hughes Clarke et al., 2012, 2013; Hughes Clarke, 2016; Hizzett et al., 2017). A full survey of the entire system was also undertaken every two weeks (Hughes Clarke et al., 2012). Hourly surveys were then conducted for a smaller number of days in 2012 (Hughes Clarke et al., 2014). These are by far the most numerous time-lapse bathymetric surveys yet collected for any turbidity current system. It was found that the proximal channels and associated lobes were highly active. Two types of event were defined; large-scale failures of the delta lip, and numerous events that caused bedform movement which were triggered by smaller failures of sediment settling from river plumes (Hughes Clarke et al., 2012; Clare et al., 2016; Hizzett et al., 2017).

Larger delta-lip failures

Failure of the delta-lip triggered relatively large volume events containing 2×10^4 m^3 to 15×10^4 $m^3$of sediment. Five delta-lip failures occurred over 135 days in 2011. The first two lip-failures coincided with unusually low tides, whilst the final three failures occurred a few hours after peaks in river discharge (Clare et al., 2016). This suggests that failure was triggered by unusually rapid delta-lip progradation during river discharge peaks, and

processes associated with low tides. Such processes at low tide may include expansion of gas bubbles within the sediment, or focussing of river discharge (and hence more rapid delta lip progradation) (Hughes Clarke et al., 2012, 2013; Clare et al., 2016). Sediment from the largest delta-lip failures sometimes infilled the proximal channels on the delta front. This channel fill was then reworked and resedimented by subsequent flows onto the lobes occurring beyond the channel mouths (Hughes Clarke, 2012).

Movement of bedform trains (bedform-migrating events)

A second type of event was associated with trains of crescent-shaped upslope migrating bedforms (Fig. 1B; Hughes Clarke, 2016). These asymmetrical bedforms have steep (up to 40°) downflow facing sides and flatter (<10°) upflow sides (Hughes Clarke et al., 2014). The bedform-migrating events also tended to occur when river discharges were elevated, and at lower than average tides (Hughes Clarke et al., 2014). Bedforms confined to the delta-front channels tended to have a crescentic-shaped crest that was concave in an upflow direction. Individual channelized flows caused bedform crests to migrate upflow for several tens of metres (Hughes Clarke et al., 2012, 2013). Bedform trains from the larger events continued across the lobes, where the bedforms had more sinuous crests (Fig. 1B; Hughes Clarke et al., 2012). More widely spaced bedforms are seen beyond the lobes (Fig. 3A), but no changes in bed elevation were discernable further down the basin within the resolution (*ca* 1 m) of the surveys.

Many of the bedform trains began at the delta lip, and are obviously associated with a slope failure scar near the steep delta-lip (Fig. 1B). However, almost half of the bedform-migrating events began a significant distance from the delta lip and lack an obvious failure scar

(Hughes Clarke et al., 2012, 2013; Hizzett et al., 2017). These events may be initiated by settling of sediment from the surface river plume, which forms a denser near-bed layer (Hughes Clarke et al., 2014; Hizzett et al., 2017) and not by direct plunging of the river as in a true hyperpycnal flow (Hughes Clarke, 2016). Settling from river plumes produced most events, and they include some of the most powerful turbidity currents over sub-annual time scales (Hizzett et al., 2017).

The bedform trains migrate upflow, and were thus generated by supercritical flows (Normark et al., 1980; Cartigny et al., 2014; Hughes Clarke, 2016; Hage et al., 2018). Monitoring using multibeam sonars and acoustic Doppler current profilers (ADCPs) showed that the upflow migrating, periodic bedforms within proximal channels were associated with hydraulic jumps, and thus represented cyclic steps (Hughes Clarke, 2016). The deposits of bedforms in proximal channels comprised amalgamated massive sand layers (Hage et al., 2018).

Flow observations

Descending plumes of sediment from the river mouth on occasion fed denser near-bed flows, which last for about an hour and coincided with bedform translation in the channels (Hughes Clarke et al., 2014). Heavy (24 to 36 kg) blocks were placed in the proximal channels and tracked using the multibeam system (Hughes Clarke et al., 2012, 2013). The heavy blocks moved rarely, but when moved were displaced for several hundred metres downflow (Hughes Clarke et al., 2014). This suggests that some flows were rather powerful, and may have comprised dense granular flows near the bed.

An acoustic Doppler current profiler (ADCP) located by Hughes Clarke et al. (2012, 2013) on the lobe beyond the northernmost channel (Fig. 1B) showed that 20 of the 49 events in the northern channel ran out for at least 1.5 km. Most of these events on the lobe had peak velocities in the region of 50 cm/s, but the first major delta-lip failure generated a flow with a maximum speed of 150 cm/s (Hughes Clarke et al., 2012). A typical flow at the ADCP site was 5 to 15 m thick, and lasted for around an hour (Hughes Clarke et al., 2014; Hughes Clarke, 2016).

Differences in sea floor elevation during the freshet in 2011 suggest that the southern lobe was an area of net deposition, but the other lobes were not characterized by net deposition (Hughes Clarke et al., 2012). The lack of deposition on the northern and central lobes suggests that flows were stopping before reaching the lobes or that this was mainly an area of sediment bypass.

METHODS

Sea floor morphology and changes in gradient

Swath multibeam data were collected by the Canadian Hydrographic Service over three separate surveys in 2007 and 2011. The data were gridded and analysed in Arc GIS®. Maps of sea floor gradient were used to identify changes in slope, and to identify the extent of bedforms in the mid-basin.

Piston coring

Sediment samples were collected with a Benthos piston corer onboard the Canadian Coast Guard Ship (CCGS) *Vector* over three separate surveys in 2011, 2013 and 2015. A multi-sensor core logger (MSCL) was used to acquire physical property measurements, including gamma density, magnetic susceptibility, P-wave velocity and high resolution photographs. Grain size was inferred through visual inspection. X-radiographs were collected at Simon Fraser University's Earth Science department. The geochemical composition of sediment cores was measured using an Innov-X Delta Premium (DP-6000; Olympus, Tokyo, Japan) portable X-Ray fluorescence (pXRF) mounted on a Geotek MSCL (Geotek Limited, Daventry, UK). Analysis was conducted using the mining plus mode using 40 kV and 10 kV beams for 30 seconds each. Select cores were analyzed at 1 cm or 2 cm intervals.

Deep-towed (Huntec) sub-bottom profiler data

High resolution seismic reflection data were collected by the GSC-Pacific onboard the CCGS *Vector*. Data were collected in 2013 with a deep-towed Huntec system, which consisted of a boomer source and a line-and-cone receiver (Geoforce Group, Dartmouth, Nova Scotia, Canada).

Radiocarbon dating

One conifer needle and one piece of bark from Core 105 were analyzed for ^{14}C dates (Table 2). Analyses were performed at the University of California, Irvine (Keck Carbon Cycle Accelerator Mass Spectrometry) following the procedure outlined by Southon et al. (2005). Results were calibrated using OxCal version 4.2 (Bronk Ramsey, 2009) and are reported as calibrated years (cal BP).

Excess Pb-210 profiles and dating

A sediment accumulation rate was calculated for Core 103 by means of ^{210}Pb analysis. This core was collected from the deepest part of the basin, minimizing the probability of reworking by density flows or tidal currents. Analysis was conducted by Flett Research Ltd, in Winnipeg, Manitoba, using alpha spectrometry following a modified procedure from Eakins & Morrison (1978). The sediment accumulation rate was determined by calculating the slope of log (excess ^{210}Pb) with depth, as described by Robbins (1977). It was assumed that ^{226}Ra activities are in equilibrium with supported ^{210}Pb. Two samples were analyzed for ^{226}Ra activities and these were averaged and subtracted from total ^{210}Pb activities to calculate excess ^{210}Pb activity. The ^{210}Pb disintegration constant was divided into the slope of log (excess ^{210}Pb) and provides a sediment accumulation rate in cm/yr. Dates were calculated by subtracting the estimated age from the year the cores were collected.

The sediment accumulation rate was calculated using a ^{210}Pb model that excludes data points from intervals interpreted to have been reworked. Such reworked deposits include bioturbated zones, intervals characterized by mud and sand laminations, and sand beds that are interpreted to represent instantaneous deposition. The intervals that were interpreted as instantaneous deposition (mud and sand beds) were removed from the calculation of total sediment thickness in order to achieve a sediment accumulation rate that only accounts for constant hemipelagic deposition rate, or an event-free depth (EFD).

RESULTS

Morphology of the Howe Sound system

The main Squamish River-sourced turbidite system comprises three morphological regions: channelized delta-slope consisting of channels and lobes reaching just beyond the 150 m isobath, mid-slope apron/fan reaching just beyond the Britannia Fan, and distal ponded basin that ends at the Porteau Cove Sill (Fig. 1A). These regions correspond to distinctive sections along the bathymetric profile (Fig. 2). The overall form of the bathymetric profile has a steadily decreasing slope gradient, apart from a flat section associated with a prominent convex-up bulge in the area of the first major bend in the fjord axis (Fig. 1A). From interpretation of seismic data, this bulge appears to be related to antecedent topography and not to recent deposition.

Channelized delta-slope

The proximal delta-slope is characterized by three active submarine channels that extend for 1 to 2 km to the 110 to 150 m isobaths (Fig. 1B). Down to a depth of 150 m the average slope is 6^{o}, beyond this the slope decreases to an average of 1.2^{o} (Fig. 2). The three northernmost channels are active and contain sharply-defined bedforms, which deposited amalgamated massive sand layers (Hage et al., 2018). These bedforms cause local variation in sea floor gradient, with downslope faces that range between 10° and 30° (Fig. 3A) but can reach beyond 40° (Hughes Clarke et al., 2012). The two southernmost channels on the delta are located offshore from the artificially diverted Mamquam Channel (Fig. 1B). Their relatively subdued relief indicates that they are currently abandoned and partially infilled (Fig. 1B).

Beyond the three active channel mouths, are a series of lobes defined by bedform migration on bathymetric difference maps (Fig. 1B; Hughes Clarke et al., 2012, 2013). Flow expansion at the channel mouths is accompanied by a change in average gradient from 6.0° to 2.5°. In 2011, the lobes extended to a distance of 2.0 to 2.4 km from the delta lip. The downslope boundary of the lobes is delineated by a change in bedform character from shorter to longer wavelength (Fig. 3A).

Middle section of Howe Sound (mid-slope)

This part of the system extends from the lobes to a break in slope that defines a much flatter distal basin (Fig. 1A). This mid-part of the basin is also covered by ubiquitous bedforms (Fig. 3A and B). Bathymetric difference maps failed to show any systematic changes in sea floor elevation associated with the mid-basin bedforms (Hughes Clarke et al., 2012), and such changes in elevation would thus have been less than *ca* 1 m in 2010 to 2011 (Hughes Clarke et al., 2011), however an upflow migration is observed just before Core 27 in sub-bottom image (see *Sub-bottom profiles* section). Most of this mid-basin zone has relatively subdued relief, although patterns of transverse bedforms are visible in irregular patches.

The relatively smooth relief is interrupted by several elongate depressions located on the eastern side of the basin, which have steep upslope terminations (Figs 1A, 3A and 3B). The depressions may be relicts of palaeo-channels that extended from the abandoned eastern part of the Squamish Delta.

A local area of lower gradients occurs on the western side of the system, and this flatter area lacks bedforms (Figs 1A, 2 and 3A). This shows that there is an association between steeper gradients and bedform generation. This flatter area is associated with a bulge in the

axial basin profile.

Distal ponded basin

A large change in slope from >0.4° to 0.05° defines a very low gradient distal basin (Figs 1A and 2). The basin floor lacks bedforms, which are restricted to steeper (>0.4°) slopes (Fig. 3B and C).

Britannia Creek system

The Britannia Creek system emanates from the eastern side of Howe Sound, approximately 8.5 km down-fjord from the Squamish Delta (Fig. 1C). A fan-delta is located immediately offshore of the creek, forming a cone of sediment that progrades onto the basin floor (Fig. 1C; Prior & Bornhold, 1984). This cone has gradients that reduce from 30° to 2° (Fig. 3B). The surface of the fan is characterized by three broad gullies bounded by narrow ridges, the two southernmost characterized by ridge and chute morphology (Figs 1C and 3B). At the base of the cone, the gullies transition into a 100 to 200 m wide submarine channel that turns southward over a length of approximately 1 km before petering out. The sea floor adjacent to the channel is characterized by transverse bedforms.

Slide scars on fjord walls

To the south of the fan delta, a 500 m wide ridge on the sidewall of the fjord separates the fan delta from a broad slide scar depression (Figs 1C and 3B). The headscarp for this slide is 14 m in height and forms an irregular line along the shallow fjord margin. It has an estimated volume of 1.5×10^6 m^3. Seaward of this slide scar is a broad submarine debris lobe with a blocky surface (Figs 1C and 3B). The lobe deposit has an area of 8.9×10^5 m^2. Individual blocks are up to 10 m across (Prior & Bornhold, 1986). There are several other slide scars on the east fjord wall and Porteau Cove Sill (Figs 1A and 3C).

Deposit types (lithofacies) in sediment cores

Five main types of deposits are identified in this study and are summarized in Table 3 and illustrated in Figs 4 to 7. Lithofacies 1 consists of mud and sand laminations that are plane parallel or wavy/sub-parallel and thinner than 1 cm. Lithofacies 2 comprises of thin (up to 10 cm) sand beds that are generally sharp based fining up to mud or sandy tops. Lithofacies 3 sand beds are thick (up to 1 m), generally sharp-based, well sorted and fine up to muddy or sandy tops. Lithofacies 4 comprises of hemipelagic mud ranging from sandy mud to clay-rich. Lithofacies 5 are clast-rich debris flow deposits that are massive with high clay content and mud rip-up clasts. Finer grained intervals were often rich in gas due to high organic carbon content. Depressurisation during core recovery led to gas expansion and voids in the cores, which were removed from the core logs for the purposes of this analysis.

Sub-bottom profiles

Upper slope

The upper slope is generally characterized by poor acoustic penetration due to abundant sand and shallow gas. Bedforms are common and in places upflow migration can be inferred (Fig. 8). High amplitude reflections are discontinuous and cannot be correlated between bedforms.

Mid-slope

The mid-slope has acoustic penetration up to 20 m below the sea floor. The upper-mid-slope down to a depth of 200 mbsl is characterized by pervasive bedforms resulting in discontinuous high amplitude reflections (Fig. 9). Just north of Core 27 bedforms are observed migrating upflow by 25 m with a vertical increase of approximately 1.5 m (Fig. 9B).

The flat margin of the slope, at roughly 230 mbsl, is characterized by reflections are parallel and continuous (Fig. 10). At 250 mbsl the sea floor is irregular and the surface is draped with at least 3.5 m of parallel reflections with no indication of upslope migration. Below this depth resolution is poor, likely due to gas blanking.

Distal ponded basin

The basin consists of flat, parallel-bedded reflections that form a layer-cake stratigraphy (Fig. 11). The repetitive reflections fill a 30 m interval over a transparent unit interpreted as a mass transport deposit (MTD). The acoustic signal is generally attenuated at the MTD, but in places there appears to be more parallel reflections beneath (Fig. 11B). The Britannia Fan on the east side of the basin only has coverage by two Huntec lines. The sparse acoustic data show an irregular surface and very poor sub-bottom penetration indicating sandy sediments.

The lobate slide deposit south of Britannia Fan extends 1 km west from the base of the fjord wall and is between 2 m and 5 m in thickness (Figs 1C and 11A). The unit has a chaotic acoustic character with no traces of internal structure. The top is irregular with metre-scale blocks draped by a very thin layer of recent sediment.

Several other MTDs are identified interfingering with the regular parallel bedding of the ponded basin at its southern end (Fig. 11B). These units share the same chaotic acoustic properties as the debris-flow unit (Lithofacies 5) sampled in Core 32 (Fig. 4). These are likely to be debris-flow deposits originating from the glaciomarine sediment on the Porteau Cove Sill or the east fjord wall. Several large scallop shaped escarpments serve as evidence for a large amount of failed material on the north side of the sill which may account for the larger MTDs (Fig. 3C). The largest deposit is also the oldest observed in seismic record and extends

5 km to the north, where its seismic character is obscured due to gas blanking. This unit is roughly 10 m thick where an upper and lower surface are visible. There are two smaller stacked MTDs above the large MTD which extend just over 1 km to the north and are 2 to 3 m thick. Multiple small slide scars are apparent on the east fjord wall (Fig. 3C); however, the Huntec record that extends along the fjord axis is 500 m or more from the east fjord wall and shows no expression of run out from these events.

Correlation of sediment cores to sub-bottom acoustic stratigraphy

Channelized delta-slope - Acoustic penetration is poor in much of this area due to the high sand content (Fig. 8). Sediment cores within the channel and lobe deposits reveal thick bedded sand (Lithofacies 3), in the case of cores 160 and 161 penetration was limited to 1.5 m maximum consisting of medium sand (Fig. 5).

Mid-slope – The presence of repetitive thin and fine sand beds (Lithofacies 2) and thick fine to medium sand beds (Lithofacies 3) in cores confirms that the high amplitude reflections are indeed sand deposits (Figs 5 and 9). On the upper mid-slope as far down-fjord as Core 163, Lithofacies 3 sand beds, including their mud tops, are a major component of the sediment record (50% or more of total sediment accumulation in cores 159 and 162). The prevalence of high amplitude reflections throughout the slope indicates that sand beds observed in cores are widespread throughout the area.

On the lower mid-slope, although reflections are generally more continuous and parallel, sand beds are still challenging to correlate between cores wherever bedforms are present (Figs 6 and 10). At this distance from the Squamish Delta the sediment record is characterized by mud and clay deposition including thick hemipelagic mud (Lithofacies 4)

intervals, frequent mud laminations (Lithofacies 1) and less frequent thin bedded sand (Lithofacies 2) that are beyond the resolution of sub-bottom profiles, as well as thick bedded sand (Lithofacies 3). Cores 33, 107, 34 and 106 returned thick bedded sand (Lithofacies 3) at depth which are interpreted as deposits from the early 1900s based on projected pXRF data (see below) (Figs 6 and 10).

Distal ponded basin – Based on sediment core interpretation, the continuous, parallel, high amplitude reflections of the ponded basin correspond to thick bedded sand (Lithofacies 3) ranging in thickness up to 1 m (Figs 7 and 11) interbedded with thicker intervals of mud (Lithofacies 4). The continuous, parallel reflections allow for correlation between cores throughout the ponded basin.

The blocky debris lobe south of the Britannia Fan was sampled in Core 32. It comprises thick chaotic, clast-rich clay (Lithofacies 5) intervals separated by hemipelagic muds (Lithofacies 4). These hemipelagite intervals may indicate multiple stages of failure (Figs 4 and 11). Alternatively this hemipelagic interval could be mud rip-up clasts. The distal part of the debris flow is covered by 63 cm of more recent interbedded lithofacies 1, 2 and 4 deposits.

Dating and age control

Geochemical signature from Britannia Creek Mine

Mining activity at the Britannia Mine left a distinct signature of anomalously high heavy metal concentrations in the fjord sediment (Drysdale, 1990). Copper and zinc are both readily detectable by means of pXRF. High concentrations of these elements occur in thick intervals in all cores analyzed (Fig. 12). Anomalously high copper concentrations occur in

tandem with zinc concentrations, with total copper amounts usually higher. In this contribution, copper is used as a proxy for all Britannia Mine heavy metals that were introduced to the Howe Sound marine depositional environment.

This study groups copper anomalies into three categories; background, medium or high (Fig. 12). Background levels include concentrations up to 80 ppm. This boundary is based on the background copper concentration of Howe Sound sediments, as determined by Thompson & Paton (1976) and as confirmed by Drysdale (1990). Medium concentrations comprise copper values from 80 to 220 ppm. High concentration copper values extend from 220 to 1805 ppm. High copper values above 220 ppm form their own distinct log-normal population, so this was selected as the boundary between medium and high groups.

Core 30 and all other down-fjord cores are characterized by thick intervals of elevated copper concentrations (Figs 1 and 12). Up-fjord of Core 30 there is no signal of elevated copper, likely due to a combination of factors: (i) transport of contaminated material from Britannia Creek did not effectively reach this far up the fjord; and (ii) higher sedimentation rates closer to Squamish Delta diluted the copper concentration and result in a thicker amount of material burying the copper unit. The base of the elevated copper interval occurs in cores at depths greater than 2 m. The elevated interval was likely deposited during the time of the Britannia copper and zinc mine activity and the base is interpreted to represent the start of mining in 1898. The upper part of these basin cores typically return to background values (Fig. 12). Disposal of active mine tailings occurred until the mine closed in 1974, with full remediation beginning in 1997. The authors thus infer that the upper approximately 10 cm to 2 m of sediment with background copper concentrations (from basin cores to mid-slope cores respectively) was deposited sometime after 1974.

Radiocarbon – distal ponded basin

Two organic samples were analyzed for radiocarbon dating (Table 2). Both samples were extracted from Core 105 from a depth of 902 cm (Fig. 7). In order to establish a depth that excludes thick instantaneously deposited event beds, an event-free depth (EFD) (Ramsey et al., 2012), sand intervals and their mud tops were subtracted from the total depth resulting in a depth of 548 cm. The calibrated age modelled from both samples is 445 ± 12 cal BP which results in a background sedimentation rate of 1.10 cm/yr.

Excess ^{210}Pb age dating – distal ponded basin

Nineteen samples were analyzed from the top 79 cm of Core 103 (ponded basin) (Fig. 13). Samples in the top 12 cm showed evidence of bioturbation and were excluded from the age model. Samples between 26 cm and 32 cm, 44 cm and at 79.5 cm were also excluded due to their proximity to event beds and a large crack in the sediment core. Removing these reworked samples results in a slope of 0.0293 and an R^2 value of 0.7998, indicating a sediment accumulation rate of 1.06 ± 0.06 cm/yr (Fig. 13).

Calculation of sedimentation rate in distal ponded basin

The radiocarbon date produces a sedimentation rate that is comparable to the ^{210}Pb sediment accumulation rate, and dates derived using the increase in copper concentrations from Britannia Creek Mine. For instance, using the exclusive ^{210}Pb method in Core 103, a date of approximately 1885 ± 7.5 years was assigned to the base of the high copper-concentration unit. This corresponds approximately to the 1898 AD start of activity at the Britannia Mine. This consistency increases confidence in the age dating, and indicates that the effect of compaction and local erosion are not significant.

The timing of major event beds over the past 100 years in the distal basin are calculated by applying the accumulation rate of 1 cm/yr obtained in Core 103 to other basin cores. The most recent basin-wide thick sand bed (Lithofacies 3) was emplaced in *ca* 1928 (Fig. 7; Table 4). The top of the debris-flow deposit (Lithofacies 5) in Core 31 (Fig. 7) has an estimated age of 1963, whilst the recurrence interval of the last four thick-bedded sands in Core 105 is *ca* 100 years. The largest basin-wide debris flow deposit (Lithofacies 5) is covered by approximately 30 m of basin fill (Fig. 11). Applying the sediment accumulation rates deduced from ^{14}C analysis at core 105 this study estimates an age of 1200 cal BP for the debris-flow deposit (Table 4).

Dating via repeat bathymetric surveys – Squamish Delta

Repeat bathymetric surveys constrain changes in sea floor elevation and hence date deposits emplaced in the last five years in proximal channels and lobes of the Squamish Delta (Hughes Clarke et al., 2012, 2013). Changes in elevation in excess of 1 m occurred during a few months in 2011, suggesting that the deposits in the 2 to 4 m long cores herein from these areas were deposited (or reworked) during the last few years. Multibeam surveys were conducted on a lower frequency of the mid-slope area by Hughes Clarke et al. (2012) and sedimentation rates are estimated to be 5 to 10 cm/yr at 200 m water depth.

Frequency of flow deposits

Flow frequency is determined using counts of flow events, which varies between different types of direct monitoring and core analysis. The number of events is most accurately measured by ADCPs with sub-minute accuracy (Hughes Clarke et al., 2012, 2013). During the 2011 survey of Hughes Clarke et al. (2012, 2013), repeat multibeam surveys were conducted every weekday, and counted 103 events in the three active delta-front channels. They may underestimate the number of events if there were flows during the weekends and if

multiple events occurred in the same channel within a few hours. The greatest uncertainty in event counts come from sediment cores, where an event was counted if there was an interval of turbidite sand or mud that is separated by hemipelagite mud. Uncertainties arise through identification of hemipelagite (although it tends to have a high biogenic component and different colour to turbidite mud). Earlier deposits may be eroded or amalgamated by later flows leading to an underestimate of events. Such erosion and amalgamation may affect the proximal lobe cores to the greatest degree. The top of the elevated copper unit served as an isochron to estimate flow frequency at different core positions. A value of 20 years is used based on the sediment accumulation at core 103 above the elevated copper interval (this time corresponds to the remediation in the 1990s). Turbidite sand and mud layers (lithofacies 1, 2 and 3) that occur above the elevated copper unit were counted by visual inspection of cores and are summarized in Table 5. Thick sand beds (Lithofacies 3) only occur in Core 30, the most proximal core analyzed with pXRF. Thin sand beds (Lithofacies 2) occur on average once each year or more in mid-slope Cores 30, 28 and 27. This number drops dramatically after the slope break that occurs mid-slope. Laminations (Lithofacies 1) tend to decrease in frequency with distance from Squamish Delta (except for Core 30 where there are fewer laminations than other cores on the mid-slope) and are deposited throughout the system.

Spatial changes and organisation of deposit types

There is a general fining and thinning of sand beds with distance from the Squamish Delta (Figs 1, 5 to 7 and 12), accompanied by a decrease in event frequency. The distal ponded basin is an exception to this, as thick-bedded sands (Lithofacies 3) in this location are thicker than some places on the mid-slope.

Channelized delta-slope – Sediment cores recovered from the northern channel and lobe comprised exclusively massive thick-bedded sands (Lithofacies 3) in the upper 240 cm below the sea floor (also see Hage et al., 2018). Lithofacies 3 beds are coarse and poorly sorted sand, containing mud rip-up clasts. Based on flow monitoring, these massive sand beds appear to be the result of supercritical flows that caused up-slope bedform migration (Hughes Clarke et al., 2012; Hughes Clarke 2016).

Mid-slope – A 40 to 80cm thick sand bed (lithofacies 3) immediately underlies the sea floor in cores from the upper mid-slope (Cores 159, 162, 163 and 29, Figs 5 and 6) indicating a recent flow. A thin Lithofacies 2 bed at the surface of Cores 28, 27 and 33 may be the distal expression of this thick bed. This deposit did not reach Core 107. The lower parts of these cores comprise of mud laminations (Lithofacies 1) and thinly-bedded sand (Lithofacies 2) interbedded with thick-bedded sand (Lithofacies 3) or hemipelagic mud (Lithofacies 4). A change in sedimentation occurs in the lower mid-slope cores (for example, Cores 107, 34 and 106, Fig. 6) where beds in the top 1 m become thinner and finer grained. Millimetre-scale mud laminations (Lithofacies 1) are frequent with some thin sand beds (Lithofacies 2). Thick sand beds (Lithofacies 3) are present at depth, and are interpreted as deposits from events in the early 1900s. Time equivalent beds were not reached in cores from the upper mid-slope. Thick bedded sands (Lithofacies 3) in slope cores generally grade from medium to fine sand and have a higher degree of sorting than the channelized delta-slope and sometimes contain mud rip-up clasts.

Ponded basin – Cores from the flat, distal basin mainly comprise thicker intervals of hemipelagic mud (Lithofacies 4) than on the slope with fine-grained laminations (Lithofacies 1, typically clay) and thin-bedded sands (Lithofacies 2) (Fig. 7). However, they also contain thicker massive or graded sand beds (Lithofacies 3), which are laterally extensive and can be

correlated between core sites. Thick sand beds (Lithofacies 3) in the basin are finer than on the slope and are better sorted with rare mud rip-up clasts.

Sources of flows

It is important to first determine the source of flows, if their spatial evolution is to be understood. Trains of bedforms that extend from proximal delta-front channels show that flows in the northerly part of the system originate from the Squamish Delta. However, the thick sand beds in the distal basin may have originated either from Squamish Delta or Britannia Fan. For three reasons the authors favour a source from the Squamish delta. First, there are continuous bedforms from the Squamish Delta down to the base of the slope, indicating that the Squamish Delta flows are capable of travelling >10 km. Second, the Squamish Delta is a large sandy system that would serve as a source for the large volume of sand required to cover the entire distal basin with up to 1 m of sand – an estimated 5 to 10 x 10^6 m^3 based on thick sand deposits (Lithofacies 3) in the basin. One of the headscarps along the southern margin of the current Squamish Delta-lip has an estimated volume of 5.9 x 10^6 m^3. The Britannia Fan is a much smaller system that lacks the volume of sediment required for the thick sand deposits throughout the basin. The large gully on the fjord wall just south of Britannia Creek has an estimated volume of only 5.8 x 10^5 m^3. Third, due to the short distance between the fan and the nearest core, Britannia Fan seems unlikely to be responsible for the deposition of such well-sorted, fine sand beds. If the first hypothesis is correct, then the most recent thick sand bed (Lithofacies 3) in the distal basin cores originated from the Squamish Delta.

DISCUSSION

This study initially outlines how the frequency and character of the flows varies with distance. The main controls on flow frequency and behaviour are then discussed, focussing on: (i) whether flows ignite or dissipate; (ii) where and why flow is supercritical or subcritical; and (iii) whether flows form a gradual continuum with distance, or are bimodal. It concludes by discussing how thick beds in the distal basin may record tsunamigenic landslides, earthquakes or major floods.

Variations in flow frequency and character down the system

Proximal channels of the Squamish Delta

The proximal channels are highly active with over 100 events recorded by repeat surveys in a few months (Hughes Clarke et al., 2012, 2013). These often powerful flows (Hughes Clarke, 2016) cause substantial (up to 10 m/day) translation of 2 m high bedforms in the proximal delta-front channels (Fig. 14; Hughes Clarke et al., 2012; Hizzett et al., 2017). These bedform-displacing events are triggered by failure of the steep and sometimes rapidly prograding delta-lip, or by settling of sand from a surface plume that episodically creates denser near-bed flows (Hughes Clarke et al., 2014). Water column measurements show that the upper parts of these channel flows are relatively dilute (<0.03% sediment volume) and may be prone to lofting, but the events are driven down-slope by denser near-bed flow (Hughes Clarke et al., 2014). The character of this near-bed flow is poorly documented, but it is able to episodically transport heavy (24 to 36 kg) blocks for several hundred metres. Deposition of massive sand intervals within the channel thalweg also suggests elevated near-bed sediment concentrations (Talling et al., 2012), and this is consistent with imaging of denser near-bed layers (Hughes Clarke, 2016). These channelized flows are supercritical

and produce trains of up-slope migrating bedforms, or cyclic steps (Cartigny et al., 2011; Hughes Clarke et al., 2012, 2013, 2016; Hage et al., 2018). Some of the most powerful and longest runout events are caused by sediment settling from surface plumes, rather than slope failure, at least over sub-annual time scales (Hizzett et al., 2017)

Channel-mouth lobes

Less than half (*ca* 40%) of the often powerful channelized flows in the northern active channel reach an ADCP mooring site on the corresponding distal lobe (Figs 1B and 14; Hughes Clarke et al., 2012, 2013), which is located just *ca* 500m from the northern channel mouth. This suggests that many flows decelerate and die out within only a few hundred metres of the channel termination. The flows had speeds of 50 to 150 cm/s at the ADCP site, were 5 to 15 m thick, and lasted for about an hour (Hughes Clarke et al., 2012, 2013). The most powerful flows caused bedforms to move and were most likely supercritical as bedforms migrated upslope. At this location, flows may rapidly lose competency once they exit the confined channels and deposit their sediment load on the lobes producing thick sand beds.

Cores from the lobes show that some of the more powerful flows deposited thick massive sand beds (Lithofacies 3), and most likely had high near-bed sediment concentrations (Fig. 5). Core 157, at the ADCP site, shows repetitive thick-bedded sands (Lithofacies 3) interbedded with thin-bedded sand (Lithofacies 2) and hemipelagic mud (Lithofacies 4) (Fig. 5). The thin intervals of hemipelagic mud (Lithofacies 4) that separate sand beds probably indicate that very little time passed between events. There is likely to be some amount of erosion of hemipelagic intervals that has occurred with each powerful event, as the lobe is

mainly an area of sediment bypass (Hughes Clarke, 2016), but surveyed changes in sea floor bathymetry suggest that the lower 2 m of this core likely represents less than one summer's worth of sedimentation. This sandy sequence is buried by slower, muddy deposition during the winter months. This facies association agrees with observations from the ADCP site (Hughes Clarke et al., 2012) that showed at least 20 events over the summer months and a less active period before May and after August.

Mid-slope

Thin deposits dominate the mid-basin cores with some thick-bedded sands (Lithofacies 3), especially proximal to the lobes (Figs 6 and 14). Cores 159 to 34 range in distance from 1.0 to 7.5 km from the channel mouths (Figs 5 and 6). There is a down-fjord transition from thick-bedded sands (Lithofacies 3) near the lobes to predominantly thin sand and mud laminations (Lithofacies 1) with thick intervals of hemipelagic mud (Lithofacies 4). The deposition of very thick sand beds (Lithofacies 3) with mud rip-up clasts at Core 159, 1 km from the channel mouths, indicates that some of the more powerful flows observed on the lobe deposit also reach this distance. The transition is rather pronounced at Core 30, located 2 km away from the channel mouths, where there are only three thick sand beds (Lithofacies 3) but many thin sand beds (Lithofacies 2) (Fig. 5). This transition indicates that at this short distance beyond the lobes most flows were relatively weak and fine-grained. This rather abrupt transition is somewhat surprising given the powerful (up to 2 to 3 m/s) nature of flows a few kilometres up-slope, in the proximal channels and lobes. All slope cores show a record of at least one thick sand bed (Lithofacies 3), indicating occasional high concentration flows in both the upper and lower mid-slope. More widely spaced, up-slope migrating bedforms (such as those in Fig. 9B) suggest that mid-slope flows were also supercritical, although such bedforms are not developed on the flat mid-slope section.

Distal ponded basin

Flows that reached the distal basin experienced an abrupt and significant decrease in slope from *ca* 0.4° to 0.05° (Fig. 14). The lack of bedforms in the distal basin suggests a transition to subcritical flow, or flow that was too weak to generate bedforms. Mud laminations (Lithofacies 1) are common through the entire slope and extend through the flat basin indicating that dilute flows did reach the distal extent of the system. The down-fjord transition from sand beds to laminations is an indication of flow deceleration and the transition from high concentration, dense flow conditions to dilute flow conditions. The mud laminations (Lithofacies 1) probably represent the distal expression of flows from the Squamish Delta. More voluminous and powerful flows that carried sand reached the distal basin roughly every hundred years. The powerful basin plain flows deposited massive sand, and thus most likely had relatively high near-bed sediment concentrations.

Large-scale failure of the fjord walls

The most recent large-scale failure of the fjord wall to the south of the Britannia Fan produced a distinctive blocky landslide deposit with a limited lateral extent. This event is estimated to have occurred in the 1960s, a time frame where four floods occurred within four years (Table 1). Cores show that this landslide deposit comprises chaotic units of glaciomarine clay separated by silt and sand laminations indicating multiple stages of failure.

What controls down-system changes in flow frequency and character?

Where and why do flows dissipate

It has been proposed that turbidity currents may have two main types of behaviour (e.g. Parker, 1982). First, flows that erode become denser and faster, a process termed ignition. Second, flows that decelerate will tend to deposit sediment and therefore slow down even

further, a positive feedback called dissipation. A striking observation is that numerous flows die out across only a few hundred metres on the channel-mouth lobes (Figs 14 and 15; Table 5). There is a change from hundreds of powerful events per year in the proximal delta-front channels, to around 20 events per year on the lobe, to just two to five events per year on the mid slope (Figs 14 and 15). This shows that many flows dissipate rapidly over short distances, once they become unconfined. It may also be linked to the relative coarse-grained (sandy) material transported in the proximal system (Hage et al., 2018), which can settle out rapidly once flows decelerate. Some flows may ignite within the proximal channels on the delta front, but there is little evidence for ignition (increases in flow power with distance) across the lobes and mid slope. Once beyond the confined channel there is likely a dilution of flows due to sediment deposition and water entrainment (Cartigny et al., 2011). Flow dilution has been linked to decreasing slopes elsewhere and is associated with increased bedform wavelength (Normandeau et al., 2016).

Supercritical and subcritical flow

There is ongoing debate about the relative importance and extent of supercritical and subcritical flow in turbidity currents. Recent work has proposed that supercritical flows are commonplace (e.g. Postma & Cartigny, 2014; Covault et al., 2016) and that it is recorded by up-slope migrating bedforms in many locations worldwide (Symon et al., 2016). There appear to be two scales of up-slope migrating bedforms in global compilations; coarse bedforms in confined channels, and finer-grained bedforms on unconfined slopes (Wynn et al., 2002; Symons et al., 2016).

In Howe Sound, it is apparent that upslope migrating bedforms (and therefore supercritical flow) are widespread both in the proximal channels and on the unconfined mid-slope. Supercritical bedforms in proximal channels are coarser grained and form amalgamated massive sand layers (Hage et al., 2018), whilst those on the mid slope are both finer-grained and thinner bedded. There is a strong correlation between supercritical flow and sea floor gradient (Fig. 13). Up-slope migrating bedforms are generally absent on gradients of <0.4° degrees, which occur in flatter parts of the mid-slope and in the distal basin (Fig. 3). There is often a sharp termination to zones characterized by pervasive up-slope migrating bedforms, where sea floor gradient undergoes a major change from *ca* 0.4° to 0.05°. This may be the location of a transition from subcritical flow via a hydraulic jump (Postma et al., 2009; Covault et al., 2017). If this is the case, these hydraulic jumps are not associated with discernable sea floor scours – as has been suggested to be the case in other locations (Macdonald et al., 2011; Dorrell et al., 2016).

Are flow frequency and character bimodal?

Flow frequency declines continuously from the delta front to the mid slope, but it appears to be distinctly bimodal in the distal basin. The first mode is represented by frequent laminated muds (Lithofacies 1), formed by dilute flows from the Squamish Delta at a rate of about one flow each year. These flows appear to be the distal parts of events coming from the Squamish Delta, whose frequency decreases with distance. The second mode comprises much thicker-bedded sands (Lithofacies 3), which are emplaced roughly every 100 years in the distal basin (Fig. 7). Their volume suggests that these mega-beds are mostly sourced from distinctly larger scale failures on the Squamish Delta (see section on *Sources of flows*).

Previous work has suggested that submarine canyon systems experience two scales of event, which either fill or flush the canyon and may be related to different triggering mechanisms (Arzola et al., 2008; Allin et al., 2015). Similar bimodality of flows occurs in this fjord-delta system.

Delta avulsion, system adjustment and origin of thick sands

The Squamish River underwent a major avulsion in 1971 due to a training dyke (Hickin et al., 1989). The seabed records evidence of lengthier channel systems that are now infilled, which are associated with that pre-avulsion Mamquam channel mouth (Fig. 1B). It is possible that the system is still adjusting to the avulsion that occurred 45 years ago, and channel systems may continue to grow. This can be determined by further time lapse sea floor mapping.

A cluster of deeply buried thick sands occur in the lower parts of Cores 34 and 106 in the mid slope (Figs 1 and 6). It might be proposed these thick sands were deposited near the mouth of an older and more extensive channel system. However, the dating for this study suggests that these sands pre-date the 1971 avulsion of the Squamish River, so their significance is uncertain. The 1971 river avulsion cannot explain the most recent thick sand layers (Lithofacies 3) in the distal basin (Fig. 7) which was emplaced in *ca* 1924.

Significance of large-magnitude events for geohazards

Did the most recent large landslide produce a thick sand bed?

The most recent blocky landslide deposit is clearly imaged by the deep-towed sub-bottom profiler, and the adjacent core from the distal basin can be compared to this reflection stratigraphy (Core 32; Figs 7 and 11). This comparison shows that the last major landslide,

occurring at an estimated date of 1963 on the fjord wall, is more recent than the last major sand bed in the distal basin. This sand bed is therefore not a record of the last major landslide. This suggests that not all large failures are recorded by basin-wide mega-beds, which has important implications when using mega-beds to infer frequencies of basin-margin failures, tsunami and earthquakes (Piper et al., 1999; Goldfinger, 2011; Atwater et al., 2014).

Are there links between thick sand beds and tsunamis, or other hazards?

It is important to understand whether larger-volume events in the last 100 years have generated dangerous tsunamis. One large volume thick sand bed (Lithofacies 3) and the blocky debris flows (Lithofacies 5) from just south of the Britannia Fan were emplaced in the last 100 years. The margins of Howe Sound have been populated in the last 100 years, but no tsunamis have been reported. Therefore, these larger-volume events do not appear to have produced noteworthy tsunamis. The debris-flow deposit south of Britannia Fan has a volume sufficiently large to have potentially been tsunamigenic (comparable in volume to tsunamigenic slides in Kitimat, Canada and Statland, Norway (Golder Associates, 1975; Glimsdal et al., 2016). An interval of hemipelagic mud (Lithofacies 4) in Core 32 occurs between thick intervals of chaotic debris flow deposition (Lithofacies 5) (Fig. 4) suggesting that the fjord wall slide did not occur as a single event, but probably occurred in a sequence of retrogressive failures involving smaller volumes than the total debris lobe. If the hemipelagic interval is a mud rip-up clast, however, single event volumes would be much larger.

The effect on the coastal infrastructure must also be considered in the discussion of large magnitude landslides. Delta-lip failures in 2011 have volumes ranging from 20 to 150,000 m^3 (Hughes Clarke et al., 2012) and these events produced no tsunami risk to infrastructure. The sand layers in the distal basin have volumes (5 to 10 x 10^6 m^3) that are one or two orders of magnitude larger, and may pose a larger tsunami hazard.

Much older buried MTDs are apparent in the distal basin (Fig. 11B). These deposits have similar acoustic character to the debris-flow unit (Lithofacies 5) which, in Core 32 was shown to be a chaotic clay unit. Of the buried MTDs, one is orders of magnitude larger than the others and has an areal extent that appears to cover the ponded basin (Fig. 11B). The lateral extent, volume and origins of this giant slide deposit are unclear at this time, but based on the few acoustic lines available the large slide is thickest in the south suggesting possible origins from the Porteau Cove Sill. This large event is estimated to have occurred approximately 1200 cal BP based on application of radiocarbon sedimentation rates from Core 105. Two smaller MTDs are stacked above, both of which are much smaller in scale but may be of similar origin (Fig. 11B).

Do thick sand beds in the distal basin record major earthquakes?

It has been suggested that large turbidites may be a record of major earthquakes, which trigger large slope failures (Piper et al., 1999; Goldfinger, 2011). However, the last major slope failure appears to have not generated a thick sand bed (Lithofacies 3) and the last thick sand bed does not correspond to a major earthquake. Two major earthquakes have occurred in the last *ca* 100 years (Table 1) and, at most, only one of these earthquakes could be linked to a thick sand bed (Lithofacies 3). The M7.3 Courtenay earthquake of 1946 was felt in Victoria and Vancouver; however, an earthquake of this magnitude is not expected to

have had much effect on sediment stability at distances greater than 100 km from the epicentre (Rogers, 1980). The last megathrust earthquake on the Cascadia Subduction Zone occurred in 1700. At Core 105 in the distal basin there is one very thick sand bed (Lithofacies 3) at 6.5 m below sea floor that roughly corresponds to this date (*ca* 1671 ± 20.4 based on application of the 1 cm/yr sediment accumulation rate that is approximately agreed between ^{210}Pb in core 103 and ^{14}C in core 105 to EFD of Core bed 1; Table 4). The sand bed is 95 cm thick, which is 30 cm thicker than other thick sand beds (Lithofacies 3) in the core. However, it is uncertain whether this thick sand bed (Lithofacies 3) is related to seismic forcing and further analysis is required. This increased thickness could be the result of multiple stages of failure, or could be related to a basin resonance effect where the turbidity current is reflected off the fjord walls or the Porteau Cove Sill (Lamb et al., 2006; Toniolo et al., 2006; Patacci et al., 2015).

SUMMARY AND CONCLUSIONS

There are few studies to have monitored turbidity currents in action, and even fewer studies that have linked flow observations to deposits. This article provides one of the most complete studies yet of a turbidity current system that extends from source to sink, and which combines monitoring, deposits and shallow seismic data. This study in Howe Sound shows how the frequency and character of flows changes with distance, and provides insight into what controls those changes. The proximal part of the system is highly active, with more than 100 events in channels that extend for *ca* 1.5 km across the delta front. These flows are often powerful (2 to 3 m/s), with around half of the flows reaching the lobes. However, once these flows become unconfined they tend to dissipate rapidly over a few

hundred metres. This results in only one to five flows per year on the mid slope, which extends up to 8 km from the delta front (Table 5). Upflow migrating bedforms show that supercritical flow is widespread on gradients >0.4°, both within confined proximal channel and on the unconfined lobes and mid-slope. A sharp decrease in slope from 0.4° to 0.05° separates the mid-slope from a distal basin floor, where flow was most likely subcritical. The distal basin has two scales of flow deposit (laminations and mega-beds) that indicate that flows were bimodal. Thick sand mega-beds (Lithofacies 3) in the distal basin most likely record unusually large mass wasting events on the Squamish Delta, which occurred on average every 100 years over the past 500 years. However, the most recent large fjord wall failure does not appear to have produced a basin-wide mega-bed or noteworthy tsunami. This study therefore provides new insights into what control turbidity current frequency and dissipation, where flows are supercritical or subcritical and, in this case, the limited extent to which distal mega-beds record tsunamigenic slides or large earthquakes.

ACKNOWLEDGEMENTS

The authors would like to thank the following groups for their assistance with this research: Audrey Dalimore and Royal Roads University for the use of their multi sensor core logger which collected all core images and pXRF data; Shahin Dashtgard at Simon Fraser University for the use of their X-ray laboratory; Camilia Watts, Joshua Allin and Will Symons at the University of Southampton for assisting with core logging; and Brendan Smithwick, Kirsten Matheson, Ken Cable and Izaiah Shereen for assistance with core logs and mapping. We also thank the captains and crew of CCGS Vector and CCGS John P. Tully. We also wish to acknowledge the perceptive and very useful comments from reviewers Stephen Hubbard, Joris Eggenhuisen, Bill Arnott, Marco Patacci and Alexander Normandeau and Associate Editor Jaco Baas. Funding for this project has been provided by Natural Resources Canada (Contribution #20170026) and Transport Canada. Talling was funded by NERC International Opportunities Fund grant (NE/M017540/1) on 'Coordinating and pump-priming international efforts for direct monitoring of active turbidity currents and global test sites', and NERC Infrastructure and Natural Hazards grant (NE/N012798/1) on 'What threat do turbidity currents and submarine landslides pose to strategic submarine telecommunications cable infrastructure?'

REFERENCES

Adams, J. (1990) Paleosesimicity of the Cascadia Subduction Zone: Evidence from turbidites off the Oregon-Washington Margin. *Tectonics,* **9**(4), 569-583.

Allin, J.R., Hunt, J.E., Talling, P.J., Clare, M.E., Pope, E. and **Masson, D.G.** (2016) Different frequencies and triggers of canyon filling and flushing events in Nazaré Canyon, offshore Portugal. *Mar. Geol.*, **371**, 89-105.

Arai, K., Naruse, H., Miura, R., Kawamura, K., Hino, R., Ito, Y., Inazu, D., Yokokawa, M., Izumi, N., Murayama, M. and **Kasaya, T.** (2013) Tsunami-generated turbidity current of the 2011 Tohoku-Oki Earthquake. *Geology*, **41**, 1195-1198.

Armstrong, J.E. (1981) Post-Vashon Wisconsin Glaciation, Fraser Lowland, British Columbia. *Geological Survey of Canada Bulletin,* **322**, 1-34.

Arzola, R.G., Wynn, R.B., Lastras, G., Masson, D.G. and **Weaver, P.P.E.** (2008) Sedimentary features and processes in the Nazaré and Setúbal submarine canyons, west Iberian margin. *Mar. Geol.,* **250**, 64–88.

Atwater, B.F., Carson, B., Griggs, G.B., Johnson, H.P. and **Salmi, M.S.,** (2014). Rethinking turbidite paleoseismology along the Cascadia subduction zone. *Geology,* **42**, 827–830.

Azpiroz-Zabala, M., Cartigny, M.J.B., Talling, P.J., Parsons, D.R., Sumner, E.J., Clare, M.A., Simmons, S.M., Cooper, C. ***and*** **Pope, E.** (2017). Newly recognized turbidity current structure can explain prolonged flushing of submarine canyons. *Science Advances* **3**: e1700200.

Bornhold, B.D., Ren, P., and **Prior, D.B.** (1994) High-frequency turbidity currents in British Columbia fjords. *Geo-Mar. Lett.*, **14**, 238-243.

Buckley, J.R. (1977) *The currents, winds and tides of northern Howe Sound.* Ph.D. Thesis, University of British Columbia, Vancouver, British Columbia, p. 246.

Carter, L., Gavey, R., Talling, P. J. and **Liu, J. T.** (2014) Insights into submarine geohazards from breaks in subsea telecommunication cables. *Oceanography,* **27**(2), 58-67.

Cartigny, M.J.B., Postma, G., Van den Berg, J.H. and **Mastbergen, D.R.** (2011) A comparative
study of sediment waves and cyclic steps based on geometries, internal structures and numerical modelling. *Mar. Geol.*, **280**, 40-56.

Cartigny, M.J.B., Ventra, D., Postma, G. and **Van den Berg, J.H.** (2014) Morphodynamics and
internal structures of bedforms under supercritical-flow conditions. *Sedimentology*, **61**, 712-748.

Church, M. and **Miles, M.J.** (1987) Meteorological antecedents to debris flow in southwestern
British Columbia; some case studies. *Geol. Soc. Am. Rev. Eng. Geol.*, **3**, 63-79.

Clare, M.A., Talling, P.J., Challenor, P., Malgesini, M. and **Hunt, J.E.** (2014) Distal turbidite records reveal a common distribution for large (> 0.1 km3) submarine landslide recurrence. *Geology*, **42**, 263-266.

Clare, M.A., Hughes Clarke, J.E., Talling, P.J., Cartigny, M.J. and **Pratomo, D.G.** (2016) Preconditioning and triggering of offshore slope failures and turbidity currents revealed by most detailed monitoring yet at a fjord-head delta. *EPSL*, in press.

Cooper, C., Wood, J. and **Andrieux, O.** (2013) Turbidity current measurements in the Congo Canyon. OTC 23992. Offshore Technology Conference, 6-9 May, Houston, Texas. 12 pp.

Covault, J.A., Kostic, S., Paull, C.K., Sylvester, Z. and **Fildani, A.** (2017) Cyclic steps and related supercritical bedforms: Building blocks of deep-water depositional systems, western North America. *Marine Geology*. 393, 1 November 2017, 4-20.

Crookshanks, S. and **Gilbert, R**. (2008) Continuous, diurnally fluctuating turbidity currents in Kluane Lake, Yukon Territory. *Can. J. Earth Sci*., **45**, 1123-1138.

Dorrell, R.M., Peakall, J., Sumner, E.J., Parsons, D.R., Darby, S.E., Wynn, E., Ozsoy, E. and **Tezcan, D**. (2016) Flow dynamics and mixing processes in hydraulic jump arrays: Implications for channel-lobe transition zones. *Marine Geology*, **381**, 181-193.

Drysdale, K. (1990) *Geochemistry of a buried marine mine tailings deposit, Howe Sound, British Columbia.* MSc thesis, University of British Columbia, Canada, 375 pp.

Eakins, J. D. and **R. T. Morrison** (1978) A new procedure for the determination of lead-210 in lake and marine sediments. *International Journal of Applied Radiation and Isotopes,* **29**, 531-536.

Ellis, D.V. and **Popham, J.D.** (1983). Accidental formation and the subsequent disappearance of a contaminated beach : a case history of environmental management. In *Sandy Beaches as Ecosystems* (A Machlachlan & T. Erasmus. Eds), pp.719-776.

EVS Environmental Consultants (1997) Summary and overview of environmental effects of the Anaconda Britannia Mine on juvenile salmonids and the marine environment in Howe Sound, report to Environmental protection department, Environment Canada.

Golder Associates (1975) Report to B.C. Water Resources Service on investigation of seawave at Kitimat, B.C..*Tech. Rep. 9/87*, B. C. Water Resource Service, Vancouver, B. C., Canada.

Goldfinger, C., Morey, A.E., Patton, J.R., Nelson, C.H., Johnson, J.E., Witter, R.C., Priest, G.C., Wang, K., Zhang, Y.J. and **Beeson, J.** (2010) Supercycles: evidence of clustering and holocene history of energy management from the long cascadia paleoseismic record. Abstract AGU Chapman Conference on Giant Earthquakes and Their Tsunamis, Chile, May 2010.

Goldfinger, C. (2011) Submarine paleoseismology based on turbidite records. *Ann. Rev. Mar. Sci.*, **3**, 35-66.

Glimsdal, S., L'Heureux, J.S, Harbitz, C.B. and **Løvholt, F.** (2016) The 29th January 2014 submarine landslide at Statland, Norway—landslide dynamics, tsunami generation, and run-up. Landslides, **13** (6), 1435–1444.

Hage, S., Cartigny, M.J.B., Clare, M.A., Sumner, EJ., Vendettuoli, D., Hughes Clarke, J.E., Hubbard, S., Talling, P.J., Lintern, D.G., Stacey, C.D., Englert, R.G., Vardy, M.E., Hunt, J.E., Yokokawa, M., Parsons, D.R., Hizzett, J.L., Azpiroz-Zabala, M. and **Vellinga' A.J**. (2018). How to recognize crescentic bedforms formed by supercritical turbidity currents in the rock record: insights from active submarine channels. Geology, in review.

Heezen, B.C. and **Ewing, B.C.** (1952) Turbidity currents and submarine slumps, and the 1929 Grand Banks earthquake. *Am. J. Science,* **250**, 849-873.

Hickin, E.J. (1989) Contemporary Squamish River sediment flux to Howe Sound, British Columbia, *Can. J. Earth Sci.*, **26,** 1953-1963**.**

Hill, P.R. (2012) Changes in submarine channel morphology and slope sedimentation patterns from repeat multibeam surveys in the Fraser River delta, western Canada. In: *Sediments, Morphology and Sedimentary Processes on Continental Shelves: Advances in technologies, research and applications* (Eds M.Z. Li, C.R. Sherwood, and P.R. Hill), *Int. Assoc. Sedimentol. Spec. Publ.,* **44**, 47-70.

Hizzett, J. L., Hughes Clarke, J. E., Sumner, E. J., Cartigny, M. J. B, Talling, P. J. and **Clare, M. A.** (2017). Which triggers produce the most erosive, frequent and longest runout turbidity currents on deltas? *Geophysical Research Letters*, **45**, 855-863.

Hughes Clarke, J.E., Brucker, S., Muggah, J., Church, I., Cartwright, D., Kuus, P., Hamilton, T., Pratomo, D. and **Eisan, B.** (2012) The Squamish ProDelta: Monitoring Active Landslides and Turbidity Currents. *Canadian Hydrographic Conference 2012*, Proceedings, 15pp.

Hughes Clark, J.E., Brucker, S., Muggah, J., Hamilton, T., Cartwright, D., Church, I. and **Kuus, P.** (2012) Temporal progression and spatial extent of mass wasting events on the Squamish prodelta slope. In: *Landslides and Engineered Slopes: Protecting Society through Improved Understanding* (Ed. E. Eberhardt, C. Froese, K. Turner, and S. Leroueil) pp. 1091-1096. Taylor & Francis Group, London.

Hughes Clark, J.E., Videra Marques, C.R. and **Pratomo, D.** (2014) Imaging active mass wasting on a fjord delta, Squamish, British Columbia. In: *Submarine Mass Movements and Their Consequences VI* (Eds S. Krastel, J-H. Behrmann, D. Volker, M. Stipp, C. Berndt, R. Urgeles, J.D. Chaytor, K. Huhn, M. Stasser, C.B. Harbitz), *Springer, Advances in Natural and Technological Hazards Research,* **37**, 249–260.

Hughes Clarke, J.H. (2016) First wide-angle view of turbidity currents links migrating cyclic steps to flow characteristics. *Nature Comm.* **7**, 11896.

Hunt, J.E., Wynn, R.B., Talling, P. J. and **Masson, D. G.** (2013) Turbidite record of frequency and source of large volume (>100 km3) Canary Island landslides in the last 1.5 Ma:

Implications for landslide triggers and geohazards. *Geochemistry, Geophysics, Geosystems*, **14**, 2100–2123.

Inman, D. L., Nordstrom, C. E. and **Reinhard, E.F.** (1976) Currents in submarine canyons: An air-sea-land interaction. *Annu. Rev. Fluid Mech.,* **8**, 275–310.

Lamb, M.P., Toniolo, H. and **Parker, G. (2006)** Trapping of sustained turbidity currents by intraslope minibasins. *Sedimentology*, **53**, 147-160.

Lintern, D.G., Hill, P.R. and **Stacey, C.** (2016) Powerful unconfined turbidity current captured by cabled observatory on the Fraser River delta slope, British Columbia, Canada. *Sedimentology*, **63**, 1041-1064.

Liu, J.P., Liu, C.S., Xu, K.H., Milliman, D.D., Chiu, J.K. Kao, S.J. and **Lin, S.W.** (2008) Flux and fate of small mountainous rivers derived sediments into the Taiwan Strait. *Mar. Geol.,* **256**, 65-76.

Macdonald, H.A., Wynn, R.B., Huvenne, V.A.I., Peakall, J., Masson, D.G., Weaver, P.P.E. and **McPhail, S.D.** (2011) New insights into the morphology, fill, and remarkable longevity (>0.2 m.y.) of modern deep-water erosional scours along the northeast Atlantic margin. *Geosphere*, **7** (4), 845-867.

Mountjoy, J.J., Howarth, J.D., Orpin, A.R., Barnes, P.M., Bowden, D.A., Rowden, A.A., Schimel, A.C.G., Holden, H., Horgan, H.J., Nodder, S.D., Patton, J.R., Lamarche, G., Gerstenberger, M.,
Micallef, A., Pallentin, A. and **Kane, T.** (2018). Earthquakes drive large-scale submarine canyon development and sediment supply to deep-ocean basins. *Sci. Adv*. **4**: eaar3748

Nilsen, T.H., Shew, R.D., Steffens, G.S. and **Studlick, J.R.J.** (2008) *Atlas of deep-water outcrops (Eds.),* pp.66. AAPG Studies in Geology, Boulder, Colorado.

Normandeau, A., Lajeunesse, P., Poiré, A.G. and **Francus, F.** (2016) Morphological expression of bedforms formed by supercritical sediment density flows on four fjord-lake deltas of the south-eastern Canadian Shield (Eastern Canada). *Sedimentology,* **63**(7), 2106-2129.

Normark, W.R., Hess, G.R., Stow, D.A.V. and **Bowen, A.J.** 1980. Sediment waves on the Monterey Fan levee: a preliminary physical interpretation. *Mar. Geol.*, **37**(1–2), 1–18.

Parker, G. (1982) Conditions for the ignition of catastrophically erosive turbidity currents. *Mar. Geol.,* **46**, 307–327.

Patacci, M., Haughton, P.D.W. and **McCaffrey, W.D.** (2015) Flow behaviour of ponded turbidity currents. *Journal of Sedimentary Research*, 85. 885 – 902.

Paull, C.K., Mitts, P., Ussler III, W., Keaten, R. and **Greene, H.G.** (2005) Trail of sand in upper Monterey Canyon. GSA Bulletin, **117**, 1134–1145.

Paull, C.K., Ussler W., III, Caress, D.W., Lundsten, E., Barry, J., Covault, J.A., Maier, K.L., Xu, J. and **Augenstein, S.** (2010) Origins of large crescent-shaped bedforms within the axial channel of Monterey Canyon. *Geosphere*, **6**, 755-774.

Piper D.J.W., Cochonat, P., and **Morrison, M.** (1999) The sequence of events around the epicentre of the 1929 Grand Banks earthquake: initiation of debris flows and turbidity currents
inferred from sidescan sonar. *Sedimentology*, **46**, 79-97.

Pirmez, C., Beaubouef, R.T., Friedmann, S.J. and **Mohrig, D.**, (2000) Equilibrium profile and baselevel in submarine channels: examples from late pleistocene systems and implications for the architecture of deepwater reservoirs. In: Deep-Water Reservoirs of the World (Ed. Weimer, P., Slatt, R.M., Coleman, J., Rossen, N.C., Nelson, H., Bouma, A.H., and Styzen, M.J.). GCSSEPM Foundation 20th Annual Research Conference, pp. 782–805.

Postma, G., Cartigny, M. and **Kleverlaan, K.** (2009) Structureless, coarse-tail graded Bouma Ta formed by internal hydraulic jump of the turbidity current? *Sedimentary Geology*, **219** (1-4), 1-6.

Postma, G. and **Cartigny, M.J.** (2014) Supercritical and subcritical turbidity currents and their deposits—a synthesis. *Geology,* **42**(11), 987–990.

Prior, D.B. and **Bornhold, B.D.** (1984) Subaqueous Delta Morphology, Britannia Beach, Howe Sound, British Columbia. Geological Survey of Canada, Open File 1096, 1984; 1 sheet, doi:10.4095/129918.

Prior, D.B. and **Bornhold, B.D.** (1986) Sediment transport on subaqueous fan delta slopes, Britannia Beach, British Columbia. Geo-Marine Letters, **5**, 217-224.

Prior, D.B, Bornhold, B.D., Wiseman, W.J. Jr, and **Lowe, D.R.** (1987) Turbidity current activity in a British Columbia fjord. *Science,* **237**, 1330–1333.

Ramsey, C.B. (2009) Bayesian Analysis of Radiocarbon Dates. *Radiocarbon,* **51**(1), 337-360.

Ramsey, C.B., Staff, R.A., Bryant, C.L., Brock, F., Kitagawa, F., van der Plicht, J., Schlolaut, G., Marshall, M.H., Brauer, A, Lamb, H.F., Payne, R.L., Tarasov, P.E., Haraguchi, T., Gotanda, K., Yonenobu, H., Yokoyama, Y., Tada, Ryuji, T. and **Nakagawa, T.** (2012) A complete terrestrial radiocarbon record for 11.2 to 52.8 kyr B.P. *Science*, **338**, 370–374.

Robbins, J.A. (1997) Geochemical and geophysical applications of radioactive lead. In: *The biogeochemistry of lead in the environment*, (Ed J.O. Nrigua) vol. 1, pp. 285-337. Elsevier/North Holland Biomedical Press, New York.

Southon, J.R., Santos, G.M., Druffel, E.R.M., Griffin, S., Trumbore, S.E. and **Xu, X.** (2005) High throughput, high precision 14C AMS with a small accelerator. Proceedings of IAEA International Symposium on Utilization of Accelerators.

Steffen Robertson and Kirsten (B.C.) Inc. and Gormely Process Engineering. (1991), *Evaluation of ARD from Britannia Mine and the Options for Long Term Remediation of the Impact on Howe Sound*, report to B.C. Acid Mine Drainage Task Force, Ministry of

Energy, Mines and Petroleum Resources.

Sumner, E.J., Siti, M.I., McNeill, L.C., Talling, P.J., Wynn, R.B., Henstock, T.J., Djajadihardja, and **Permana, H.** (2013) Can turbidites be used to reconstruct a paleoearthquake record for the
Sumatran Margin. *Geology*, **41**, 763-766.

Syvitski, J.P.M and **Murray, J.W.** (1981) Particle interaction in fjord suspended sediment. *Mar. Geol.*, **39**, 215-242.

Syvitski, J.P.M and **MacDonald, R.D.** (1982) Sediment character and provenance in a complex fjord; Howe Sound, British Columbia. *Can. J. of Earth Sci.*, **19**, 1025-1044.

Talling, P.J., Masson, D.G., Sumner' E.J. and **Malgesini, G**. (2012) Subaqueous sediment density
flows: depositional processes and deposit types. *Sedimentology*, **59**, 1937-2003.

Talling, P.J., Malgesini, G. and **Felletti, F.** (2013) Can liquefied debris flows deposit clean sand over large areas of sea floor? Field evidence from the Marnoso-arenacea Formation, Italian Apennines. *Sedimentology*, **60**, 720–762.

Talling, P.J. (2014) On the triggers, resulting flow types and frequency of subaqueous sediment density flows in different settings. *Mar. Geol*., **352**, 155-182.

Talling, P.J., Allin, J., Armitage, D.A., Arnott, R.W.C., Cartigny, M.J.B., Clare, M.A., Felletti, F., Covault, J.A., Girardclos, S., Hansen, E., Hill, P.R., Hiscott, R.N., Hogg, A.J., Hughes Clarke, J., Jobe, Z.R., Malgesini, G., Mozzato, A., Naruse, H., Parkinson, S., Peel, F.J., Piper, D.J.W., Pope, E. 1, Postma, G., Rowley, P., Sguazzini, A., Stevenson, C.J., Sumner, E.J., Sylvester, Z., Watts, C. and **Xu, J.** (2015) Key future directions for research on turbidity currents and their deposits. *J. Sed. Res.,* **85**, 153-169.

Thompson, J.A.J. and **McComas, F.T.**, (1974) *Copper and zinc levels in submerged mine tailings at Britannia Beach, BC*. Pacific Environment Institute.

Thorne, P.D., Hurther, D. and **Maote, P.D.** (2011) Acoustic inversions for measuring boundary layer suspended sediment processes. *J. Acoust. Soc. Am.,* **130 (3)**, 1188-1200.

Toniolo, H., Lamb, M. and **Parker, G**. (2006) Depositional Turbidity Currents in Diapiric Minibasins on the Continental Slope: Formulation and Theory. *Journal of sedimentary research*, **76**, 783-797.

Traykovski, P., Geyer, W.R., Irish, J.D. and **Lynch, J.F.** (2000) The role of wave-induced density-driven fluid mud flows for cross-shelf transport on the Eel River continental shelf, *Cont. Shelf Res.,* **20**, 2113–2140.

Wolman M.G. and **Miller JP.** (1960) Magnitude and frequency of forces in geomorphic processes. *J. Geol.,* **68,** 54–74.

Wynn, R.B. and **Stow, D.A.V.** (2002) Classification and characterisation of deep-water

sediment waves. *Mar. Geol.,* **192**, 7-22.

Xu, J.P., Swarzenski, P.W., Noble, M. and **Li, A.** (2010) Event-driven sediment flux in Hueneme and Mugu submarine canyons, southern California. *Mar. Geo*. **269** (1-2), 74-88.

Xu, J.P., Barry, J.P. and **Paull, C.K.** (2013) Small-scale turbidity currents in a big submarine canyon. *Geology,* **41**, 143–146.

Zeng, J.J., Lowe, D.R., Prior, D.B., Wiseman, W.J. and **Bornhold, B.D.** (1991) Flow properties of turbidity currents in Bute Inlet, British Colombia. *Sedimentology,* **38**, 975–996.

FIGURE CAPTIONS

Figure 1. (A) Bathymetric map of upper Howe Sound showing the entire shore to sink turbidite system from the Squamish Delta to the Porteau Cove sill (bathymetry data from Howe Sound is from 2007; active Squamish Delta front including channels is from 2011). Red dots show numbered core locations. Red line shows location of bathymetry profile in Fig. 2. Black lines show locations of Huntec sub-bottom profiles in Figs 8 to 11. Black star denotes ADCP monitoring station of Hughes Clarke et al. (2012, 2013). (B) Blow-up of Squamish Delta multibeam bathymetry showing relict channels, active channels with crescentic bedforms, lobe deposits with sinuous bedforms and wide spaced bedforms beyond the lobe deposit. (C) Blow-up multibeam bathymetry of the lower mid-slops and distal ponded basin including the Britannia Fan and location of the Britannia Mine which disposed of copper and zinc-rich mine tailings into Howe Sound from 1898 to 1974. Fjord wall slide scars and the large debris lobe are outlined.

Figure 2. Bathymetric profile and changes in average sea floor gradient along Howe Sound (location on Fig. 1). Numbered core positions shown above the bathymetric profile. The profile is broken into zones based on changes in gradient, with average gradient of each zone indicated. Red line shows position of ADCP mooring of Hughes Clarke et al. (2011). Yellow bar at base of figure indicates extent of bedforms, whilst grey bar denotes absence of bedforms.

Figure 3. Map of sea floor gradients of the upper part of Howe Sound. Bathymetry data from Howe Sound is from 2007; active Squamish Delta front including channels is from 2011. Red dots show core locations. Black dashed line shows bathymetric profile in Fig. 2. (A) Channelized margin of the delta slope and the upper mid-slope showing transition from short to long wavelength bedforms. (B) Transition from continuous bedforms on the lower mid-slope to the distal ponded basin that is flat and featureless. Bedforms are pervasive on Britannia Fan and the debris lobe has a blocky morphology. Recent slide scars correspond to debris lobes that are visible at the sea floor. (C) In the distal ponded basin the east fjord wall and Porteau Cove Sill show older slide scars that have little to no surface expression at the sea floor.

Figure 4. Core photographs, X-radiographs and graphic logs of Cores 30, 32 and 105 (positions shown in Fig. 1). Lithofacies are represented by L1-5. Internal structures are shown in photographs and X-radiographs: (A) internal laminations (Core 30); (B) inclined bedding (Core 32); (C) chaotic structure (Core 32); and (D) bioturbation (Core 105).

Figure 5. Logs of cores from locations on: (A) the proximal delta-front channel and lobe; and (B) the upper part of the mid-slope. See Fig. 1 for core locations, and Table 2 for description of facies 1 to 5. Cores are shown with increasing distance from Squamish Delta.

Figure 6. Logs of cores from locations on the mid-slope. See Fig. 1 for numbered core locations, and Table 2 for description of facies 1 to 5. Cores are shown with increasing distance from Squamish Delta.

Figure 7. Logs of cores from the distal ponded basin. See Fig. 1 for numbered core locations, and Table 2 for description of facies 1 to 5. Cores are shown with increasing distance from Squamish Delta. Correlation of debris flow deposit (Lithofacies 5) shown in orange and correlation of the most recent basin-wide thick sand bed (Lithofacies 3) in blue.

Figure 8. Huntec sub-bottom profile of northern delta-front channel and lobe. See Fig. 1 for location of cores and sub-bottom profile. The seabed is characterized by pervasive bedforms. Buried bedform crests step-up toward the north-east against flow direction. Core logs are shown in Fig. 5.

Figure 9. Huntec sub-bottom profile of the upper mid-slope. (A) Bedforms are pervasive, generally of a longer wavelength than those of the channel lobes. Inset shows Core 30 (graphic log in Fig. 4). (B) Bedforms are shown with upflow migrating crests (direction of migration shown with arrows). See Fig. 1 for location of cores and sub-bottom profiles. Core logs are shown in Figs 5 and 6.

Figure 10. Huntec sub-bottom profile of: (A) lower mid-slope; and (B) transition to ponded basin. See Fig. 1 for location of numbered cores and sub-bottom profile. The seabed is characterized by pervasive bedforms on mid-slope, except for low gradient area near Cores 107 and 33. Bedforms are draped showing no evidence of upflow migration. The ponded

basin comprises sub-parallel reflectors. Core logs are shown in Figs 6 and 7.

Figure 11. Huntec sub-bottom profile of the distal ponded basin. See Fig. 1 for location of cores and sub-bottom profile. (A) Termination of the debris flow unit from the fjord wall that is penetrated by Core 32. The surface of this debris flow comprises large blocks draped by recent sedimentation. (B) The ponded basin comprises sub-parallel, high-amplitude and laterally continuous reflectors extending to great depth. Core logs are shown in Fig. 7.

Figure 12. Changes in copper content of mid-slope and ponded basin cores. See Fig. 1 for location of numbered cores. Black lines shows top and base of elevate copper interval in cores, with more uncertain boundaries shown by dashed lines. See main text for discussion of how copper anomalies are linked to activity at Britannia Mine, and how they provide age dating of cores. Shaded fill shows the debris flow deposit which has background levels of copper

Figure 13. Log (excess 210Pb) slope results in a sediment accumulation rate of 1.06 ± 0.06 cm/yr. All data points are shown, however the sediment accumulation rate excludes data from intervals that have been reworked through bioturbation or event beds (removed intervals shown in grey).

Figure 14. Summary of the key features of the Howe Sound fjord system combining results from

this study with direct monitoring of flows on proximal delta-front channels and lobes (Hughes Clarke et al., 2011, 2012, 2013; Hughes Clarke, 2016; Clare et al., 2016). Schematic diagram showing: (i) simplified sea floor morphology: ‘A’ active channels with cyclic steps; ‘B’ lobe deposits with active sinuous bedform migration; ‘C’ relict channels; ‘D’ mid-slope with continuous bedforms; ‘E’ flat mid-slope section with featureless sea floor; ‘F’ irregular seabed scours; ‘G’ lower mid-slope with continuous bedforms; ‘H’ Britannia Fan with

channel and active bedforms; ‘I’ debris flow deposit; ‘J’ flat distal ponded basin with featureless sea floor; ‘K’ fjord wall slide scars; ‘L’ Porteau Cove Sill; (II) longitudinal profile with average slope gradient and core positions; (iii) simplified graphic logs which represent changes in depositional characteristics on different basin zones with a dashed line showing change in deposition based on a 20 year post-mining interval.

Figure 15. Changes in the frequency of flows with distance from the delta crest (Table 5), subdivided by the types of Lithofacies that they produce. Data points closer than 2 km to the delta lip show flow frequency from repeat bathymetric mapping and ADCP mooring on proximal delta-front channel and lobe (from Hughes Clarke et al., 2012). Data points beyond 2 km show average annual flow frequency determined from a 20 year interval after mining from cores on mid slope and distal ponded basin.

Table 1. Year of major floods and earthquakes in the vicinity of Howe Sound (Squamish-Lillooet Regional District, 2004; Kerr Wood Leidel, 2015).

Year	Effect on environment
1906	• Transport of boulders, avulsion near apex of Britannia Fan • Destructive flooding in Squamish River
1921	• Extreme flooding and dam breach on Britannia Creek destroyed and transported houses into Howe Sound at Britannia Beach. Transport of boulders, channel avulsion. 37 deaths • Major flooding in Squamish River, Mamquam River avulsion
1933	Partial flooding of Britannia Beach
1940	Squamish River flood caused extreme damage
1946	M7.3 Vancouver Island earthquake, 156 km west of Squamish. Substantial damage including landslides on Vancouver Island
1963	Highway washed out. Four floods within three years at Britannia and Squamish
1980	Major river floods in Squamish River and its tributaries damaged more than 200 homes. Several occurrences between 1981 and 1984 as well

1989	Failed attempt at controlled dam breach on Britannia Creek. Extensive erosion in river bed, trees transported into Howe Sound at Britannia Creek
1991	• Avulsion of fan apex, flooding at Britannia Beach • Major river floods in Squamish River and its tributaries
2001	M6.8 Nisqually earthquake 300 km south of Squamish. Local submarine slides and liquefaction
2003	Major river floods in Squamish River and its tributaries

Table 2 Radiocarbon subsample information from Core 105.

					Calibrated age (95%) [yr BP]		
Laboratory Name	Material	Depth (cm)	EFD (cm)	^{14}C age (BP)	Mean	From	To
UCI 167586	bark	902	548	355 ± 15	386 ± 44	465	315
UCI 167587	conifer needle	902	548	335 ± 15	404 ± 54	485	319
Combined		902	548		445 ± 12	467	425

Notes: Wood samples are calibrated using the IntCal13 atmospheric curve (Reimer et al., 2013).

EFD = Event Free Depth. Calibrated Age: raw calibration of the ^{14}C age.

Table 3. Lithofacies and inferred depositional processes.

Lithofacies	Lithofacies name	Bouma division(s)	Description	Interpretation of deposition process
1	Thinly (<1 cm) laminated mud and sand	Bouma Td and Te	Mud or sand laminations ranging in thickness from 1 mm to 1 cm (Fig. 4). Millimetre-scale laminations that typically occur in small groups ranging from two to five that are each separated by hemipelagic mud and often occur in association with Lithofacies 2 and Lithofacies 3 (Cores 30 and 105, Fig. 4). Laminations are typically plane-parallel, in some cases wavy and sub-parallel especially in tops of cores where bioturbation is apparent. Laminations as thick as 1 cm occur in slope cores and at depth in basin cores. Extent of bioturbation varies from negligible to extensive where only traces of primary structure remain	Weak flows that were only capable of transporting fine-grained material. Thin, fine deposits indicate dilute turbidity current (Talling et al., 2012); possibly distal expression of higher density flows that resulted in proximal Lithofacies 2 and 3 deposits
2	Thin (up to 10 cm) sand bed	Bouma Ta, Tb and Te	Fine-grained sand beds that are well-sorted or poorly sorted ranging from 1 to 10 cm in thickness (Fig. 4). Beds are generally sharp based, fining up to mud or sandy mud tops. Poorly sorted beds may have a reversely graded base, especially in cores proximal to the Squamish Delta (see Cores 29 and 28, Fig. 6). Beds that are well-sorted may have sharp, sandy top contacts, especially proximal to Britannia Fan. Plant and wood fragments are often abundant and beds may display planar laminations (Tb) or be massive (Ta). The base of Lithofacies 2 beds are typically planar and continuous, although some beds have irregular contacts, and are lenticular or discontinuous across the width of the core. Tops of beds may be slightly bioturbated showing shallow burrows	More powerful Turbidity current than Facies 1. Suppression of lamination in Ta intervals suggests high near-bed concentrations (Lowe, 1982). Planar laminated sand (Tb) can be deposited by turbidity currents with either low or high sediment concentrations (Talling et al., 2012). Mud top deposited from suspension settling with minimal current (Lowe, 1982)

3	Thick (up to 1 m) sand bed	Bouma Ta, Tb and Te	Sand beds, including associated mud top, thicker than 10 cm and as thick as 1 m (Fig. 4). Well-sorted, fine to medium grained sand with sharp base and normal gradation. Generally massive at base, sometimes showing internal laminations. Sand beds tend to fine up to mud or sandy mud tops that often have either disseminated wood fragments throughout or concentrated near the top. In basin cores with the thickest sand beds (i.e. Cores 103, 104 and 105) mud tops are often 10 cm or more and as thick as 30 cm in Core 104. The boundaries of mud tops are distinguished based on increased biogenic content of the hemipelagic unit and an associated colour change from dark to light grey. In slope and basin cores, mud rip-up clasts are sometimes present in these sand beds. Tops of beds may be slightly bioturbated showing shallow burrows	Higher density, powerful turbidity current that is relatively prolonged, and hence produces thicker sand layer. Massive structure indicates high near-bed sediment concentration. Normal grading in some layers suggests that they progressively aggraded under waning flow (Talling et al., 2012)
4	Hemipelagic mud	n/a	Hemipelagic mud shows a continuum of grain size ranging from clay-rich mud in the basin to sandy mud closer to the Squamish Delta (Fig. 4). Disseminated wood and plant fragments are common. Bioturbation is often limited to distinct intervals where burrows are visible. Bioturbation comprises extensive millimetre-scale burrows, which tend to be horizontal to sub-horizontal and may be partially overlapping. Hemipelagic mud intervals are much thicker in the distal basin, often reaching 20 cm or more in thickness. There is typically a textural contrast between hemipelagic mud and Lithofacies 1, 2 and 3 deposits where hemipelagic muds are generally finer, but may be coarser than clay-rich Lithofacies 1 deposits. There is often a sharp colour change between hemipelagic units and other units; however, the colour of Lithofacies 1 and 2 are not consistent and may be	River plume fall-out and biogenic material

			lighter or darker than hemipelagic intervals. In the interval of elevated copper concentrations, Lithofacies 4 can be distinguished from tops of Lithofacies 2 and 3 by higher copper values	
5	Clast-rich debris flow	n/a	Massive mud with high clay content and dispersed medium sand, granules and mud rip-up clasts (Core 32, Fig. 4). Defining characteristics include inclined bedding, chaotic structure and mud clasts that are typically matrix supported (Core 32, Fig. 4). Lighter colour than encasing hemipelagic mud intervals. Appears only in cores taken from the blocky debris flow lobe seen immediately south of Britannia Creek (Cores 32 and 31; Figs 1C and 7) in other places along the fjord wall. Diffuse laminations may be present at top of unit	The presence of massive clays and matrix-supported mud clasts suggests deposition from a debris flow (Talling et al., 2012). Debris flows originate from fjord wall failures

Table 4. Estimated age of major sand beds and MTDs in distal basin (based ^{210}Pb sediment accumulation rates and ^{14}C dates from cores).

Feature	Description	Date (approximate)	Dating technique
Core bed 5	Muddy debris flow (Lithofacies 5)	1963 ± 2.8	^{210}Pb Core 103 applied to Core 32
Core bed 4	Sand bed (Lithofacies 3)	1928 ± 4.9	^{210}Pb Core 103
Core bed 3	Sand bed (Lithofacies 3)	1890 ± 7.2	^{210}Pb Core 103 applied to Core 105
Core bed 2	Sand bed (Lithofacies 3)	1827 ± 11.0	^{210}Pb Core 103 applied to Core 105
Core bed 1	Sand bed (Lithofacies 3)	1671 ± 20.4	^{210}Pb Core 103 applied to Core 105 and ^{14}C core 105
Acoustic bed 1	Largest buried MTD (Lithofacies 5, Fig. 11B)	1200 cal BP (estimated)	^{14}C Core 105 projected to depth of deposit at 30 m in acoustic record

Table 5. Number and frequency of flow deposits in the last 20 years in mid-slope cores. Isochron determined using depth of burial by background level copper activities over elevated copper interval (see Figs 12 and 15). Core locations are shown in Fig. 1.

				Total number of events in last 20 years				Annual number of events per year			
Core	Distance from Squamish Delta (m)	Slope (°)	Top of copper unit (cm)	F1	F2	F3	Total	F1	F2	F3	Total
30	3200	2.5	182	40	65	2	107	2.00	3.25	0.1	5.35
28	4975	2.2	186	114	92	0	206	5.70	4.60	0.0	10.30
27	6160	2.7	173	109	22	0	131	5.45	1.10	0.0	6.55
33	6885	0.3	102	96	7	0	103	4.80	0.35	0.0	5.15
107	7146	0.3	43	82	1	0	83	4.10	0.05	0.0	4.15
34	8808	0.6	34	47	1	0	48	2.35	0.05	0.0	2.40
106	10539	0.6	11	39	0	0	39	1.95	0.00	0.0	1.95

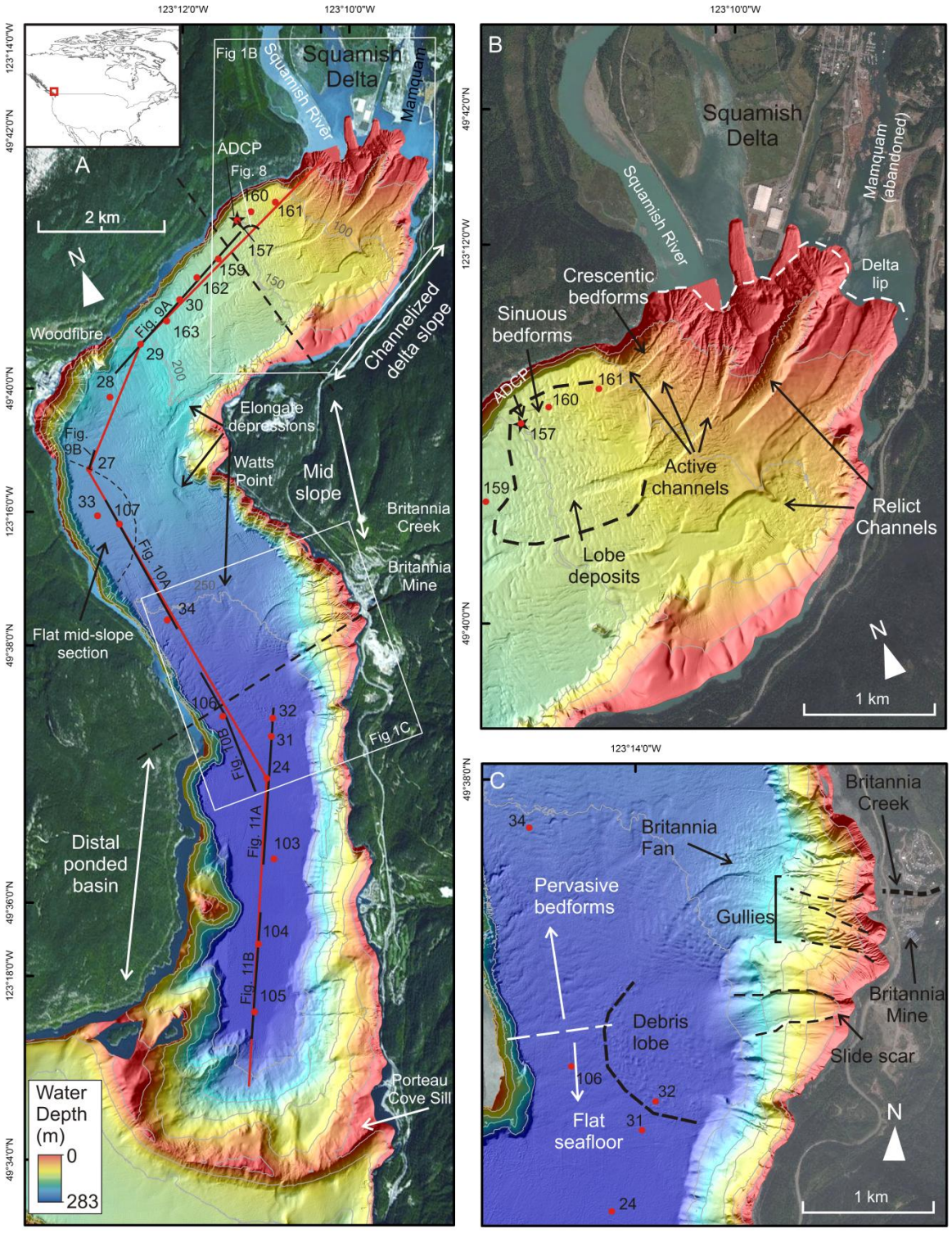

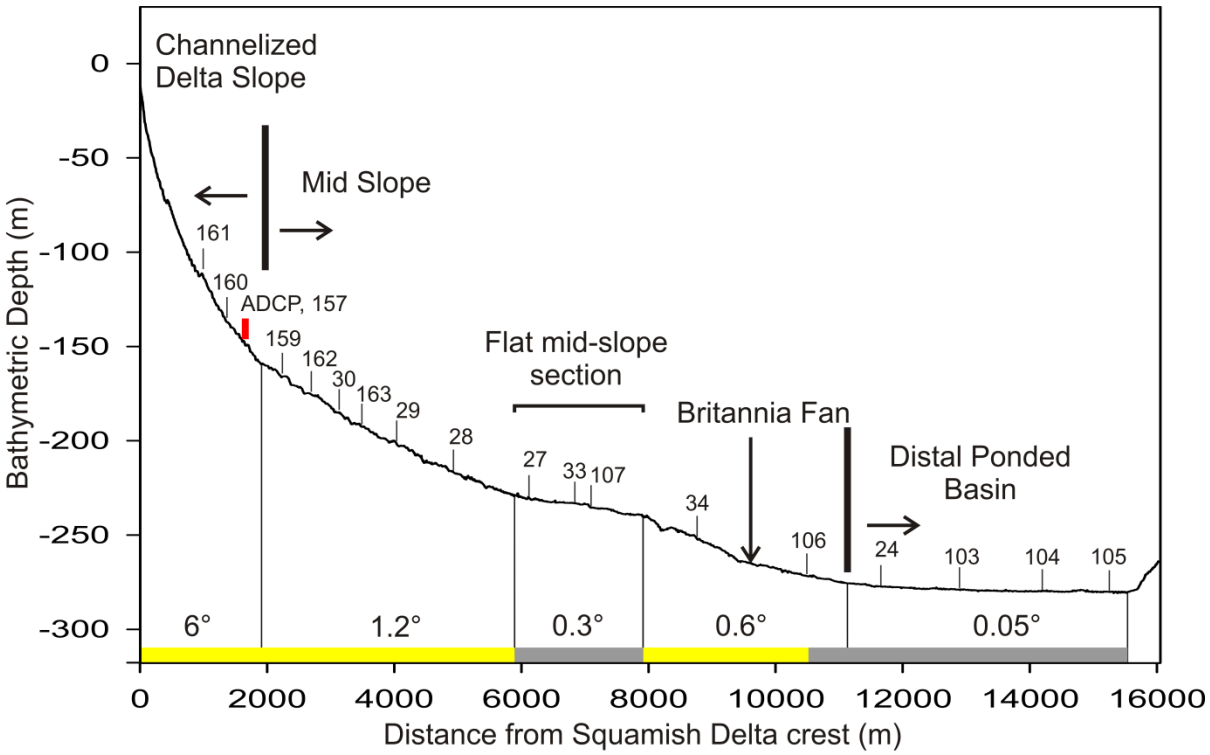

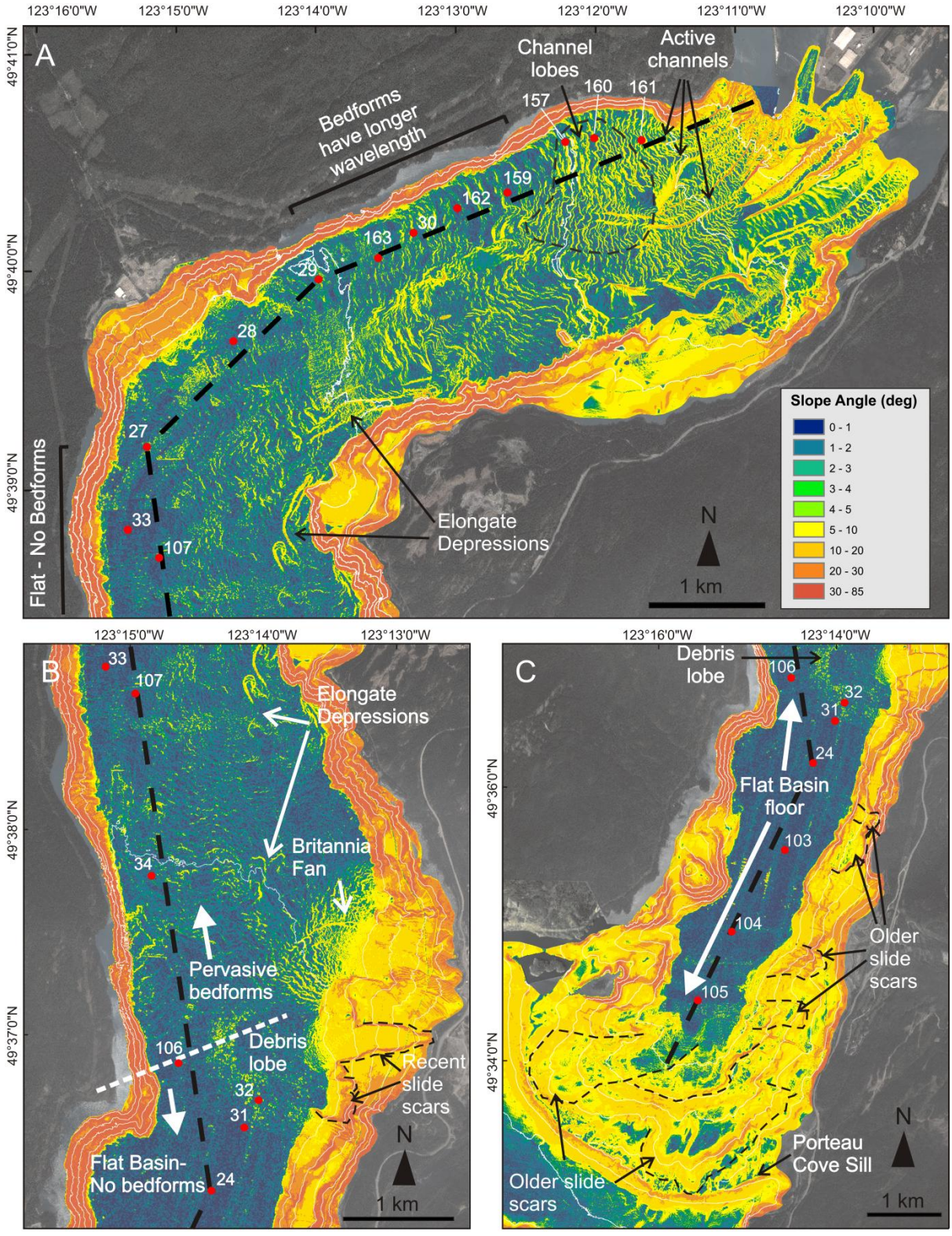

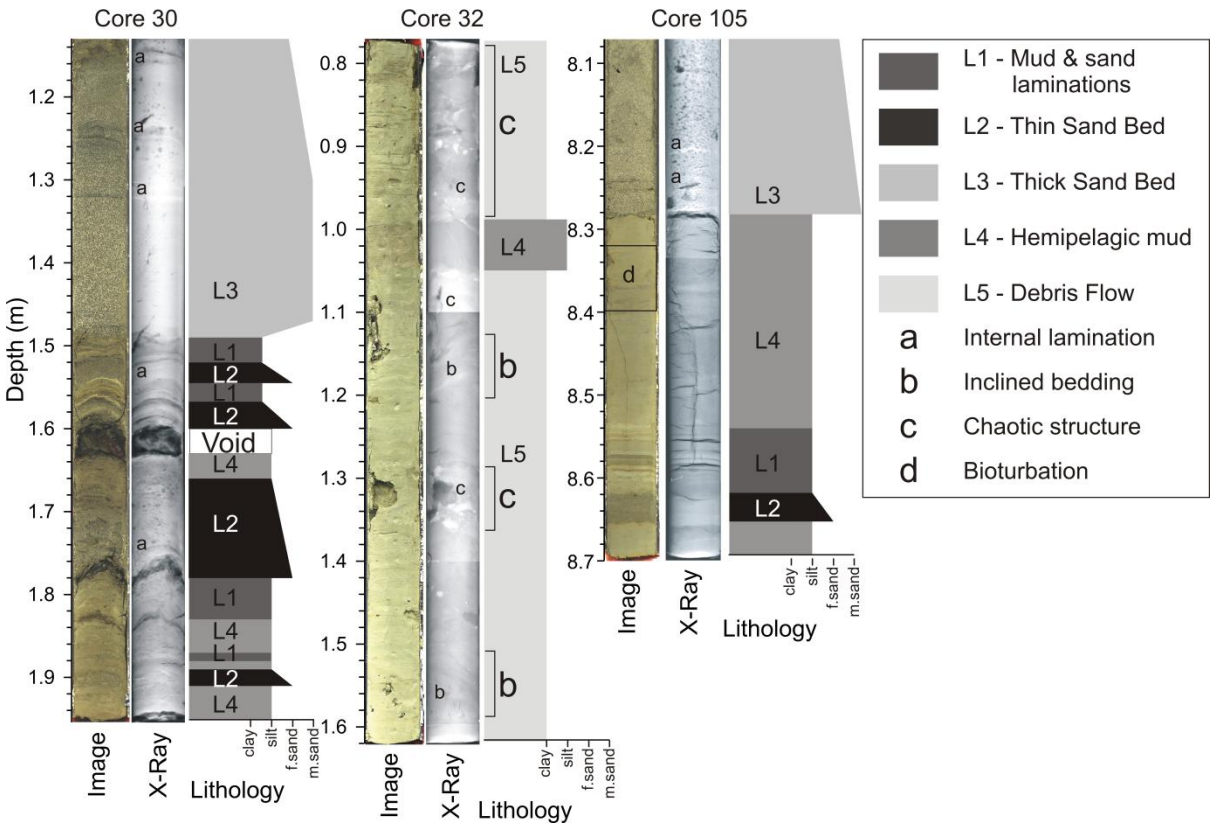

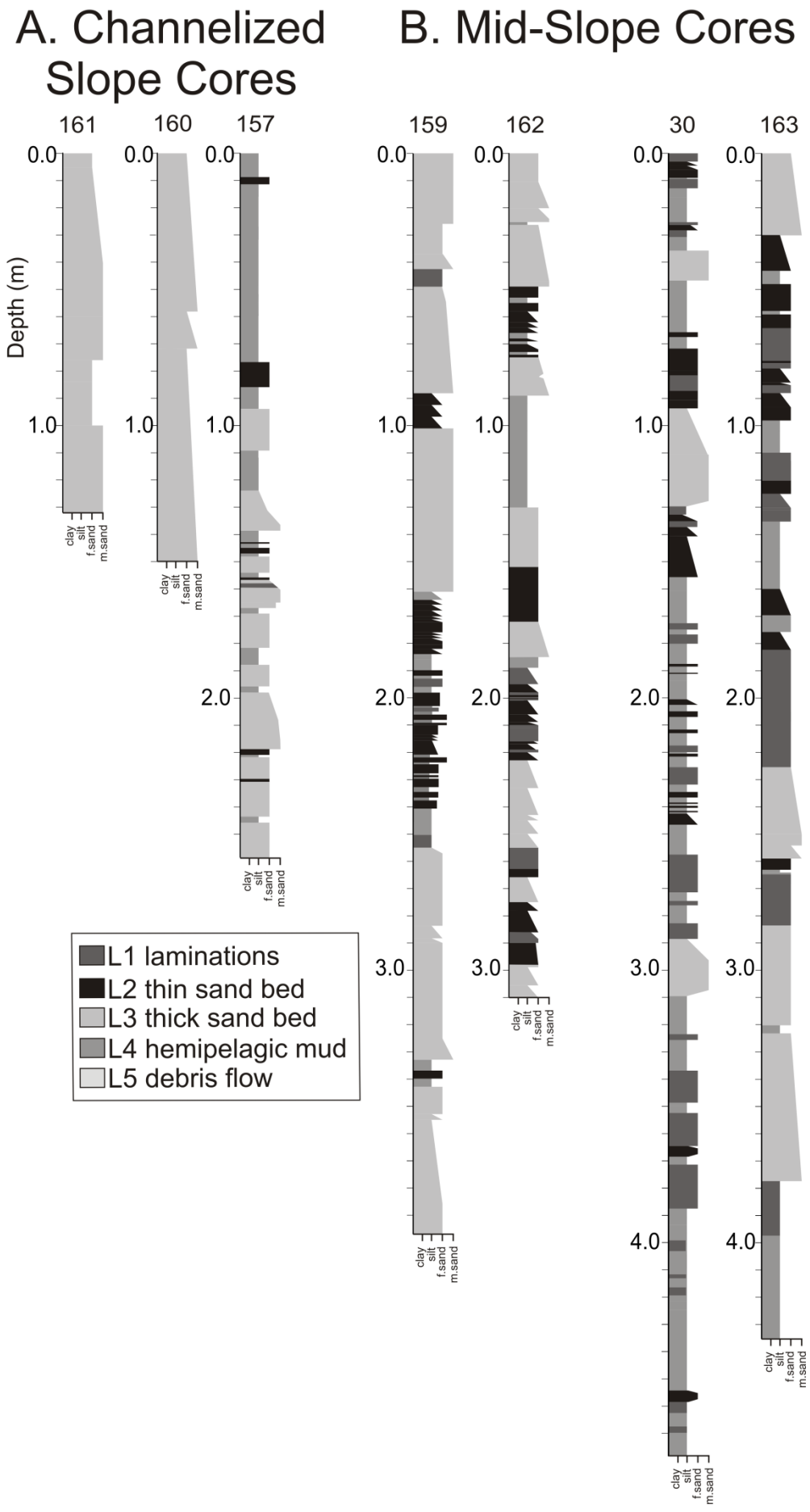

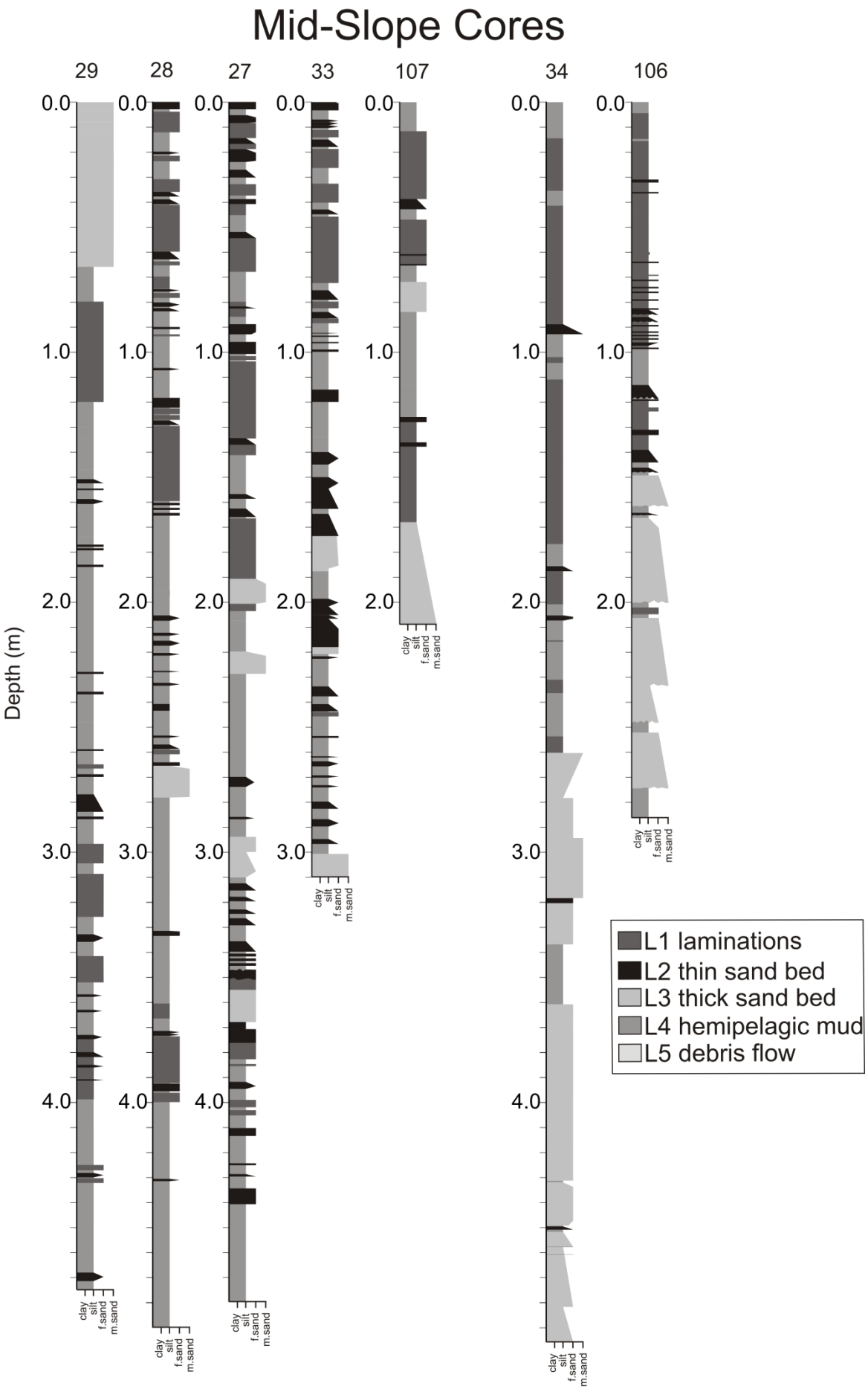

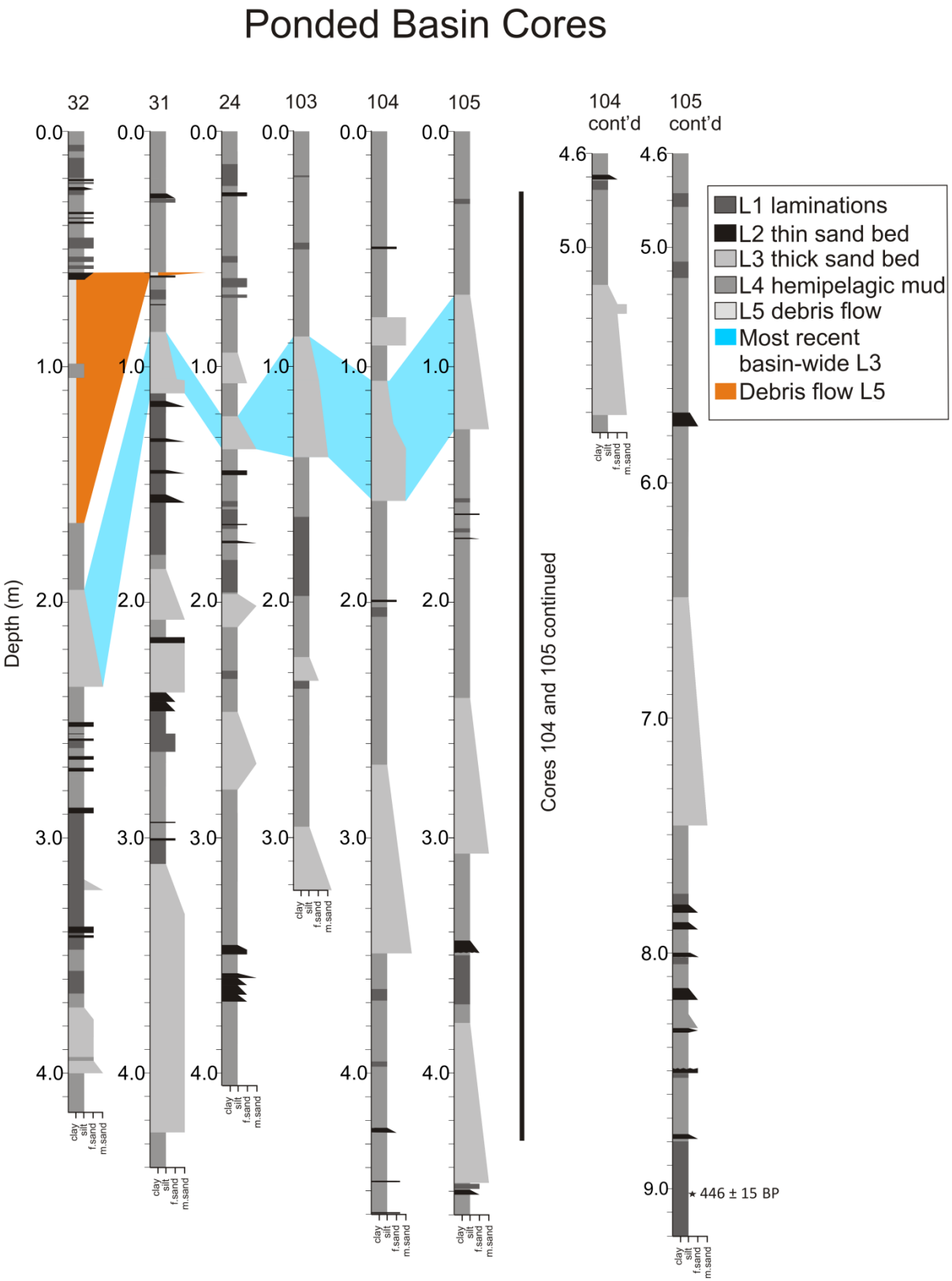

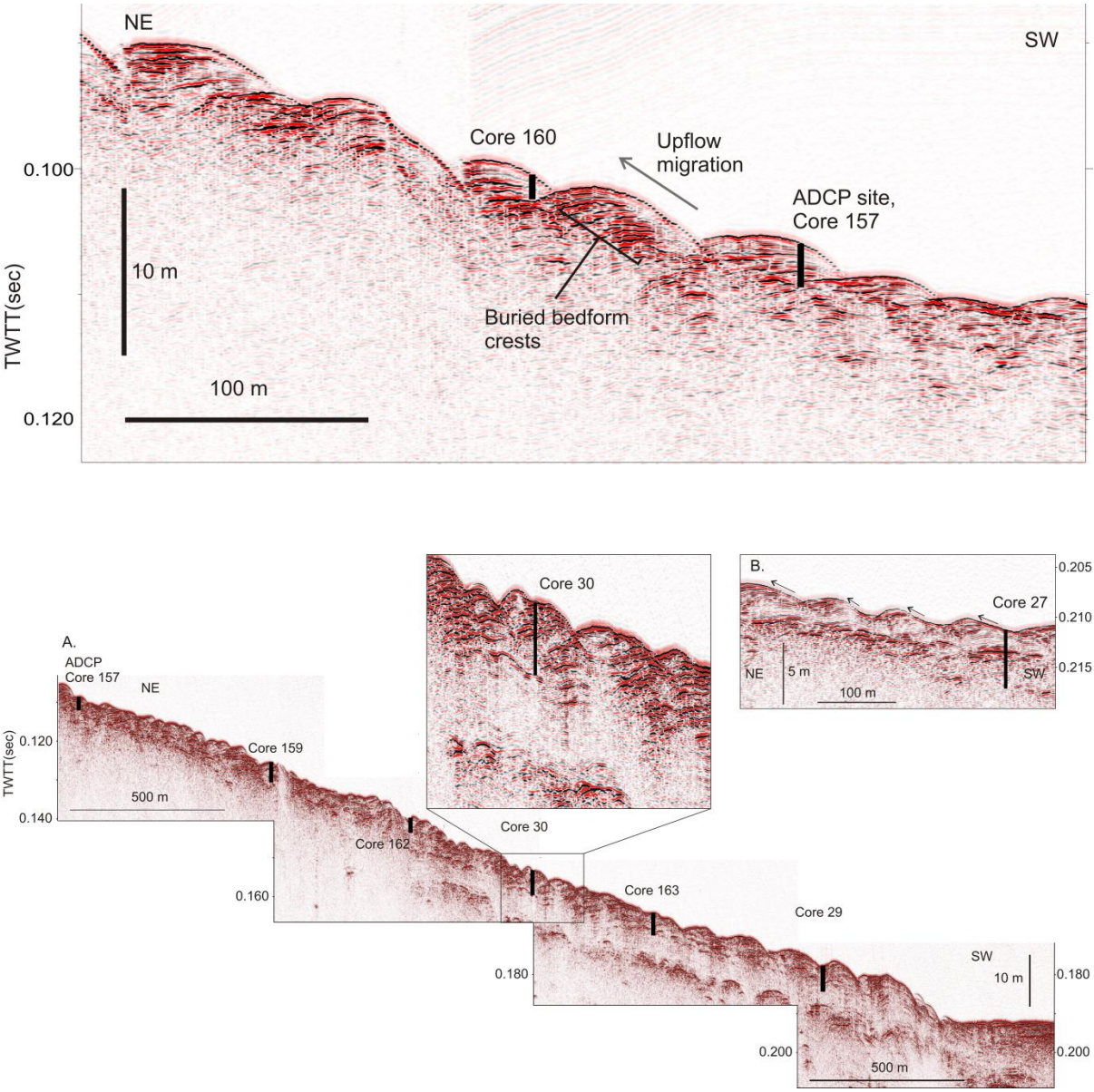

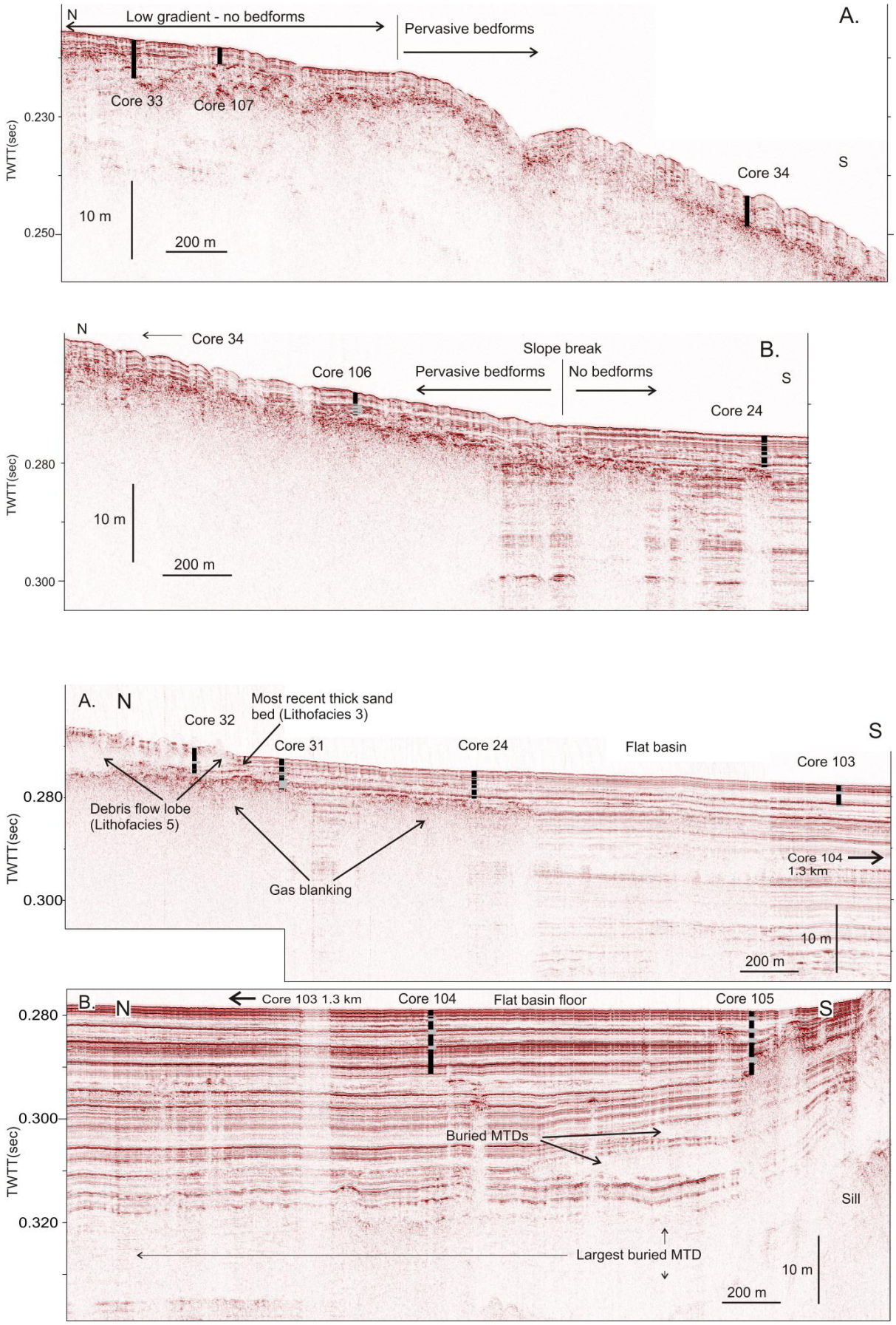

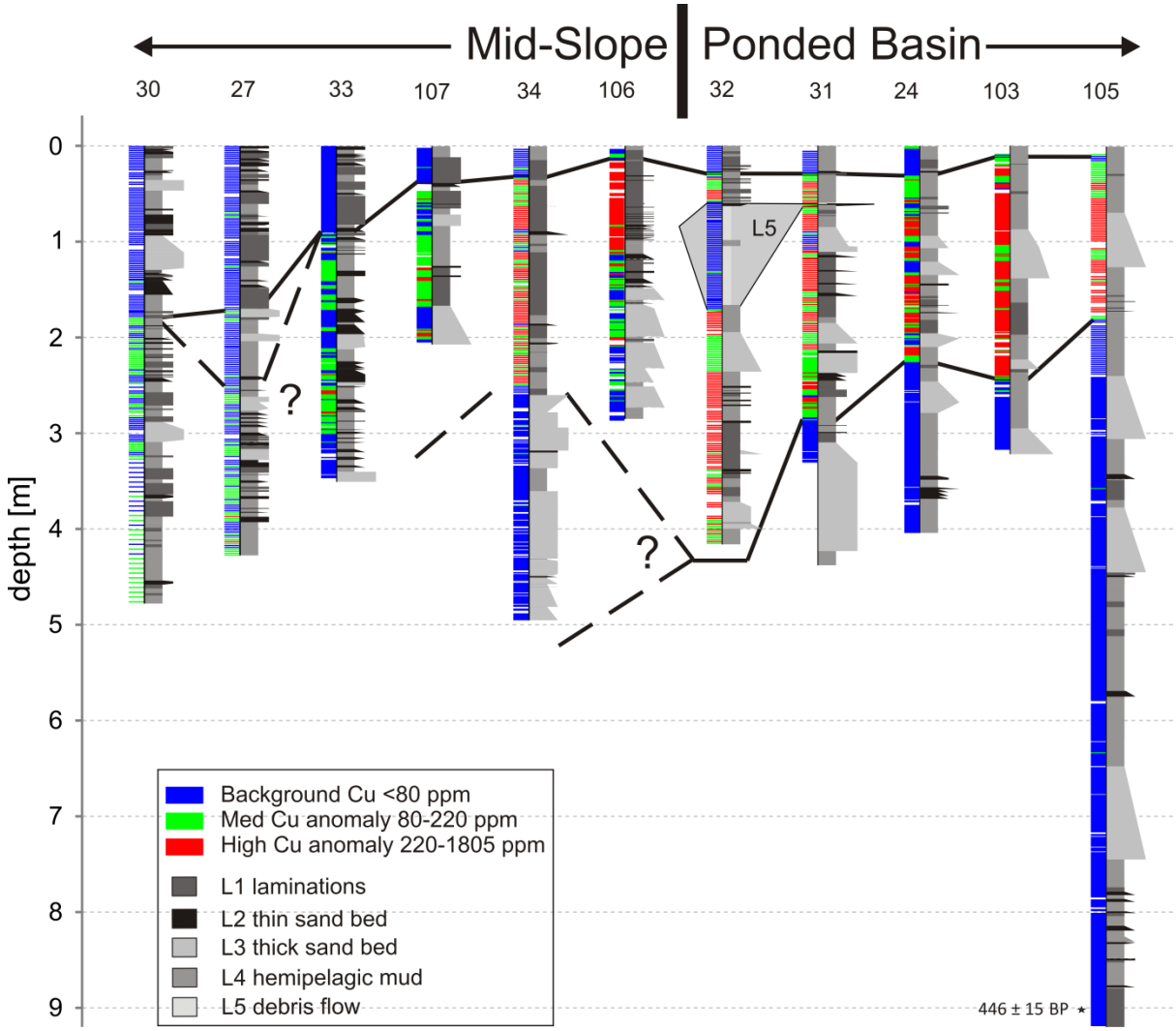

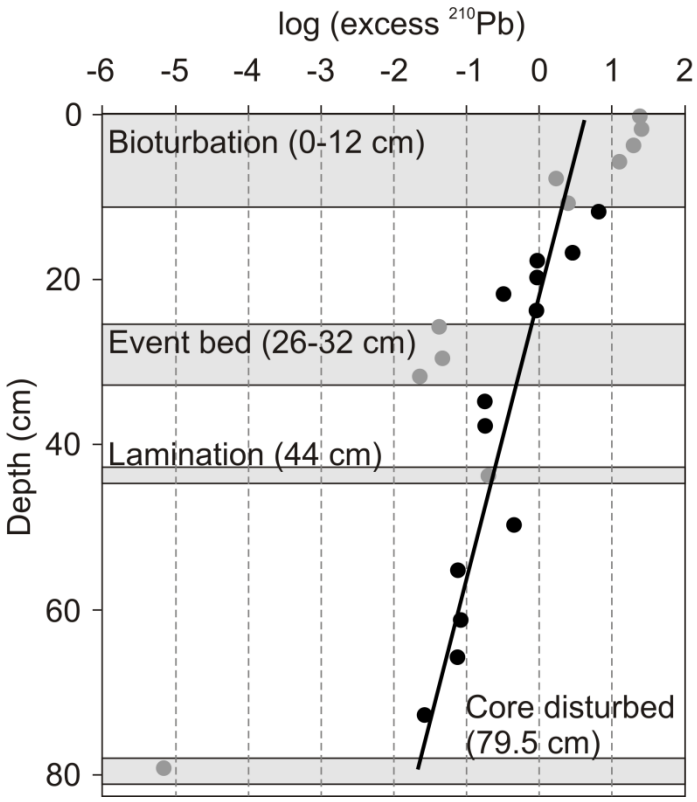

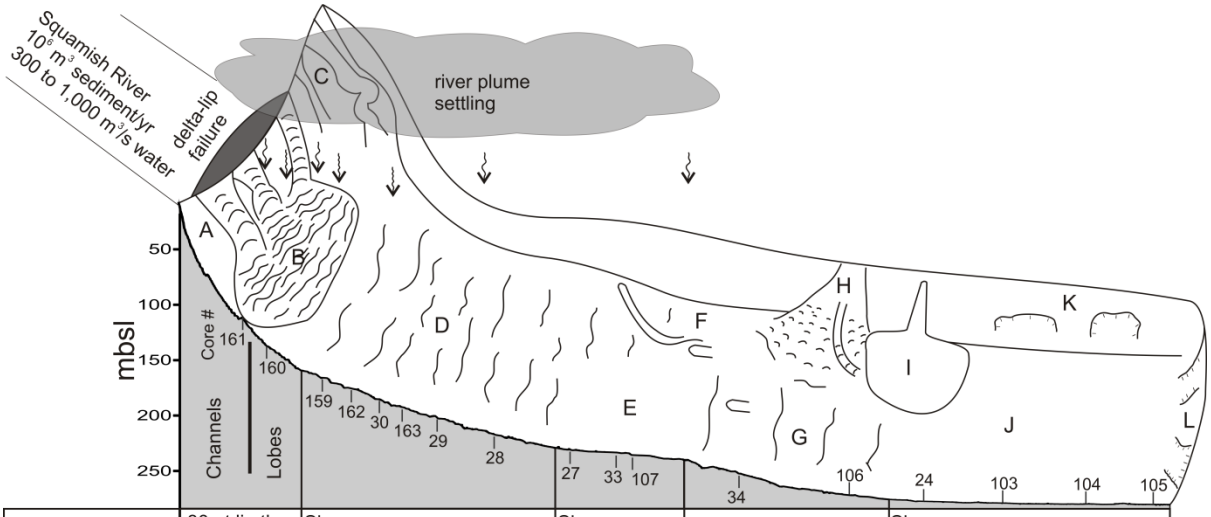

Gradient (degrees)	30 at lip then 4.7	Slope break 1.2°	Slope break 0.3°	0.6°	Slope break 0.05°
Distance from delta (Km)	2	4	6	8	10 12 14
Deposits (simplified core logs)	0 mbsf 2; 1990				
Seismic character					
Morphology	channels / lobes	unchannelised mid-slope			distal ponded basin; moraine 12 ka age
	Supercritical flow (up slope migrating bedforms) dominate, except at gradients less than 0.5°				Subcritical or weak flow: no bedforms
Event frequency	>100 flows per year; >20 flows per year; Five 10^4-10^5 m^3 lip failures / year	10 flows per year	5 flows per year	2 flows per year	1 large flow every 100 years; smaller flows more common
Sedimentation rate	elev. change >50 cm/yr				~1 cm/yr
Bedforms and dimensions	migrate upslope wavelength 20-45 m amplitude 2-5 m	migrate up-slope wavelength 50-200 m amplitude 1-2 m			flat basin floor - no bedforms
Types of data	records from flow deposits	records from flow deposits			records from flow deposits
	monitoring and bathymetric surveys	sea floor elevation changes < ~0.5 m/year (not visible in multibeam surveys)			
Triggering (Hughes Clarke et al. 2011, 2012, 2013; Clare et al., 2016)	events originating on delta front (100 events each year) (1) large-scale delta lip failure (150-50,000 m^3) (2) smaller slope failures move bedforms (< 50,000 m^3) (3) flows formed beneath settling river plume move bedforms			Flows generated by delta lip failure or river plume settling. Larger beds likely associated with failure	Large failures on Squamish Delta and fjord-wall: ~100 year recurrence interval; triggers uncertain
Direct measurement from active flows (Hughes Clarke et al. 2011, 2012, 2013; Hughes Clarke 2016)	Proximal channel: powerful (2-3 m/s) flows can move heavy (1,000 kg) objects, 3-7 m thick, short duration (<5 min). Bedform movement associated with hydraulic jumps (cyclic steps) and sometimes presence of denser near-bed layers. Lobe: flows wane to typical speeds of 50 cm/s; flows are 5-15 m thick, and last for between a few minutes and 1 hour.			none